UNIVERSIDAD DE SANTIAGO
DE COMPOSTELA
Facultad de Física
Departamento de Física Aplicada

MÁSTER EN CIENCIA Y TECNOLOGÍA DE MATERIALES

Trabajo fin de máster

Ab initio study of topological phases in perovskite bilayers grown along the (111) direction at t_{2g}^5 filling

Jose Luis Lado Villanueva
Santiago de compostela, July 2013

DECLARACIÓN DE LOS DIRECTORES

Dr. VÍCTOR PARDO CASTRO y Prof. Dr. DANIEL BALDOMIR FERNÁNDEZ declaran que:

El proyecto fin de máster titulado "Ab initio study of topological phases in perovskite bilayers grown along the (111) direction at t_{2g}^5 filling" y el trabajo presentado fue realizado por JOSE LUIS LADO VILLANUEVA bajo nuestra dirección

Víctor Pardo Castro

Daniel Baldomir Fernández

Contents

Chapter 1

Introduction

Topological insulators (TI)[1,2] are a type of materials which show a gapped bulk spectrum but gapless surface states. The topological nature of the surface states protects them against perturbations and back-scattering.[3–9] In addition, the surface of a d-dimensional TI is such that the effective Hamiltonian of its surface cannot be represented by the Hamiltonian of a d-1 dimensional material, so the behavior of a d-1 surface of a topological insulator can show completely different behavior from that of a conventional (d-1)-dimensional material. Surface states[10] can be understood in terms of solitonic states which interpolate between two topologically different vacuums, the topological vacuum of the TI and the trivial vacuum of a conventional insulator or empty space.

The ground state of a system can be classified by a certain topological number[11,12] depending on its dimensionality and symmetries present which define its topological classification.[2,13] Two-dimensional single-particle Hamiltonians with time reversal (TR) invariance are classified in a Z_2 topological class.[12] Two-dimensional TR systems with nontrivial topological index ($\nu = 1$) show the so-called quantum spin Hall effect (QSHE) which is characterized by a non-vanishing spin Chern number[14] and a helical edge current.[15] This state has been theoretically predicted and experimentally confirmed in HgTe quantum wells,[16,23,24] as well as predicted in several materials as two-dimensional Si and Ge[25] and transition metal oxide (TMO) heterostructures,.[26] These latter systems have in common that they present a honeycomb lattice structure with two atoms (A,B) as atomic basis. In that situation, it is tempting to think that the effective Hamiltonian in certain k-points could be associated to a Dirac equation. The components of the spinor would be some combination of localized orbitals in the A or B atoms,

whereas the coupling would take place via non-diagonal elements due to the bipartite geometry of the lattice. The simplest and best known example is graphene, where the low energy Hamiltonian is represented by a Dirac equation in two nonequivalent points K and K'. At half filling, graphene with TR and inversion symmetry (IS) has $\nu = 1$,[27] so a term which does not break those symmetries and opens a gap in the whole Brillouin zone would give rise to the QSHE state. The way in which an IS term can arise in a graphene Hamiltonian is due to spin-orbit coupling (SOC), however it is known that the gap opened this way is too small.[33] In contrast, a sublattice asymmetry, which breaks IS, will open a trivial gap, as in BN.[34,35]

The present work is based on the topological phases found in bilayer perovskites found by Xiao *et. al.* We will focus on the ab initio study of the behavior of two particular systems as a function of uniaxial strain and increasing on-site Coulomb interaction. To understand the result of the DFT calculations, we will also use a tight binding model to reproduce the result and identify the relevant parameters which govern the behavior of the systems.

The work is organized as follows. Firstly we will give a brief review of the relation between topological invariants and the existence of edge states giving special importance to certain toy models which allow to see that relation clearly. Also we will remember the simplest single particle models in a honeycomb lattice, which will give an intuition to understand the more complex bilayer perovskite. Secondly we will enter in the study of our particular case, both with the tight binding and DFT calculations (the main findings of this work can be found in J. L. Lado *et. al.*, arXiv:1306.2238). Finally, we will summarize the main conclusions.

Chapter 2

Topological invariants and edge states

Protected edge states in certain Hamiltonians can be related to non trivial topological invariants.[10] Broadly speaking, topology studies the relationship between mathematical objects (i.e. differential manifolds) that cannot be smoothly deformed from one to another. In this fashion, a possible question is whether a certain ground state of a Hamiltonian can be deformed into another smoothly. With smoothly we refer to find a certain path that maintains a gap opened in the system and preserving maybe a certain symmetry along the whole path.

If some system is found to sustain protected edge states, the naive argument to justify their existence is to think that locally the effective Hamiltonian is the same as in an infinite system. As an interface to a different medium is approached, the effective Hamiltonian will evolve, and if the systems are such that one fundamental state cannot be smoothly deformed into the other without closing the gap, in some point of the real space, the effective Hamiltonian will have a gapless ground state. So, topologically different vacuums would sustain irremovable edge states whose existence can be justified just for continuity reasons.

The first question that has to be answered is what are the simplest invariants that can be defined in a one particle Hamiltonian. The symmetries present in the system will determine which is the correct invariant that has to be considered to classify the ground states. We will focus in the Zak phase[18] (suitable for one dimensional systems), the Chern number[20] (for two dimensional systems, has a direct interpretation as the quantum Hall conductance[19]) and the Z_2 invariant[12] (which is defined only for Hamiltonians

with time reversal symmetry).

Secondly, we will study certain simple toy models to understand the relation between those topological invariants and the gapless edge states. Finally, a short review of the simplest phases in graphene will be given. This last part will be taken as the toy model to understand the more complex behavior of the bilayer perovskite.

2.1 Topological invariants in fermionic 2d-systems

In this section we will introduce the concept of Berry phase and Berry curvature[20] which will be useful to characterize the topological structure of the band structure of a certain system. For systems without time reversal symmetry, the number of magnetic monopoles enclosed in the Brillouin zone will be the topological invariant. For time reversal systems, the previous number is identically zero, however the existence of Kramer's degeneracy will force the existence of two states at certain points of the Brillouin zone and this irremovable degeneracy will suggest the definition of the Pfaffian matrix whose sign in all this special points will be a topological invariant. So, systems without time reversal are classified in a Z topological class whereas time reversed systems in a Z_2 class.

2.1.1 Berry phase and Berry curvature: the Chern number

Consider the reciprocal space where the Bloch states are defined. In each point of the Brillouin zone, it is defined a k-parametric Hamiltonian $H(\vec{k})$, as well as its eigenvalues $E_n(\vec{k})$ and eigenfunctions $\Psi(\vec{k})$. Focusing on a particular band of a Hamiltonian without degeneracies, the wavefunctions in each k-point have a phase degree of freedom in each point (local U(1) symmetry). Given that $H(\vec{k})$ is a smooth operator in the variable $\vec{k}$, it is possible to choose a certain phase for the wavefunctions in a local environment in such a way $\Psi(\vec{k})$ is an smooth vector in $\vec{k}$. In the same fashion as in the minimal coupling of the electromagnetic field, one can define a vector potential as

$$\vec{A} = i\langle\Psi(\vec{k})\partial_{\vec{k}}|\Psi(\vec{k})\rangle \tag{2.1}$$

which is called the Berry connection or Berry vector potential. This vector defined in the Brillouin zone is not gauge independent. This means that gauge transformation of the form

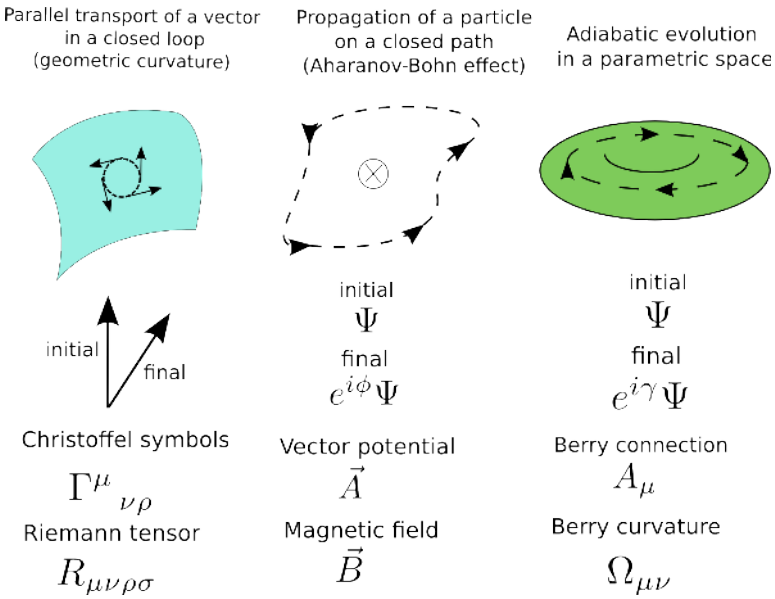

Figure 2.1: Comparison of different geometric structures that appear in physics. The first corresponds to the usual geometric curvature considered in general relativity, the second to the gauge interpretation of the electromagnetic field and the third to the geometry induced by a parametric Hamiltonian (which is the generalized version of the second one).

$$\Omega_{\mu\nu} = \partial_\mu A_\nu - \partial_\nu A_\mu \tag{2.2}$$

$$\Psi'_{\vec{k}} = e^{i\alpha(\vec{k})}\Psi_{\vec{k}} \tag{2.3}$$

induces a change in the Berry connection of the form

$$\vec{A}' = \vec{A} - \vec{\nabla}\alpha \tag{2.4}$$

In spite of this ambiguity in the Berry connection (as in the usual vector potential), the integration over a closed path is a well defined quantity given that the gauge change has to be defined in a selfconsistent way

$$\gamma = \oint \vec{A}' \cdot d\vec{k} = \oint \vec{A} \cdot d\vec{k} + \alpha(\vec{k}_0) - \alpha(\vec{k}_0) = \oint \vec{A} \cdot d\vec{k} \tag{2.5}$$

It is straightforward to define the curvature associated to the Berry connection, the so called Berry curvature.

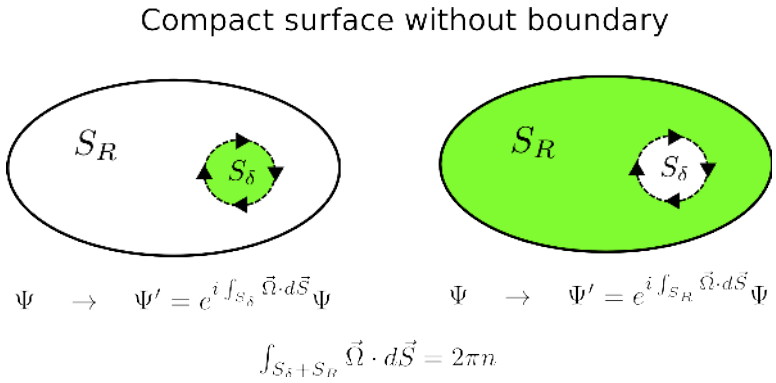

Figure 2.2: The two surfaces defined by a closed path in a closed manifold. Due to the closeness of the surface, a closed path defines two surfaces which are complementary, so in order to have a well defined adiabatic transport, the integration considered in the Stokes theorem has to be independent of the surface, which directly implies an integer Chern number.

This quantity is gauge independent (as $F_{\mu\nu}$). In three dimensions, the two index tensor can be recasted in the usual pseudovectorial form of

$$\vec{\Omega} = \vec{\nabla} \times \vec{A} \tag{2.6}$$

The previous procedure can be carried out for every parametric Hamiltonian, so the Berry curvature can be defined in cases different from Bloch Hamiltonians.

Now we will move to the simple case of two dimensional systems. The important point is that in the periodic reciprocal space, the integral of the Berry curvature in the Brillouin zone (BZ) is a quantized quantity. The proof is straightforward, a closed path divides the BZ in two parts, so the transformation that suffers the wavefunction by parallel transport can be calculated by the Stokes formula in any one as

$$\Psi \quad \rightarrow \quad \Psi' = e^{i\int_{S_\delta}\vec{\Omega}\cdot d\vec{S}}\Psi = e^{i\int_{S_R}\vec{\Omega}\cdot d\vec{S}}\Psi \tag{2.7}$$

the well-definition of the final wavefunction requires

$$\int_{S_T} \vec{\Omega}\cdot d\vec{S} = 2\pi n \tag{2.8}$$

This result is a particular case of the well known Gauss-Bonnet theorem. The integer n of the above equation is the so called Chern number. The

geometric interpretation of the Berry curvature is clear, the spectrum of the Hamiltonian induces a geometry in the parametric space. Although perturbations of the Hamiltonian will vary the eigenfunctions, so also the local curvature, the Chern number will remain constant unless a transition point is reached, where its value will change by an integer. For this reason, the Chern number is a topological invariant, i.e. a quantity that remains constant even in the presence of perturbations.

The Chern number is the so called Euler characteristic in geometry, which for two dimensional surfaces is related to their genus (their number of holes) by the formula

$$\chi = 2 - 2g \tag{2.9}$$

The physically interesting question at this point is whether certain non trivial topological structure has interesting consequences. One very clear example is the quantum Hall effect, where the Hall conductance is directly the Chern invariant.[19] This is the reason of the perfect quantization of the Hall conductance, it has a topological nature so can only take certain values which are related with the topology of the Hamiltonian.

2.1.2 The Z_2 topological invariant

Now we will focus on systems with time reversal symmetry. Even before any calculation, it is easily predictable that the Chern number has to be identically zero for these systems due to its interpretation as the quantum Hall conductance, given that σ_{xy} is odd under time reversal. So, for systems with TR symmetry, it is necessary to define another different topological index, and as it will be seen below, TR systems will be classified in a Z_2 topological class.[12] There are several approaches to define the Z_2 topological invariant, here we will give a first derivation in term of the Berry curvature and secondly the method of calculation for systems which have also inversion symmetry.[27]

For s=1/2 particles, the time reversal operator has the form

$$\Theta = e^{i\pi\sigma_y/2}K \tag{2.10}$$

where K is the conjugation operator. A Hamiltonian with time reversal symmetry will follow $\Theta^{-1}H\Theta = H$. Also, due to having $\Theta^2 = -1$, each eigenvalue shows a twofold degeneracy. This is the known as Kramer's degeneracy and the proof is straightforward. Suppose an eigenstate of H which does not have a degenerate partner $|\Psi\rangle$ so $\Theta|\Psi\rangle = \lambda|\Psi\rangle$. But $\Theta^2 = -I$

implies $\lambda^2 = -1$ which is impossible by hermiticity, so $\Theta|\Psi\rangle$ cannot be proportional to $|\Psi\rangle$ and each eigenvalue has to be twofold degenerate.

In the case of the Bloch Hamiltonian H_k the time reversal operator acts as

$$\Theta H_k \Theta = H_{-k} \tag{2.11}$$

and in the wavefunctions as

$$\Theta|\Psi_{a,k}\rangle = e^{i\chi(k)}|\Psi_{b,-k}\rangle \tag{2.12}$$

where a, b labels the two Kramer's bands. In certain k-points, the Bloch Hamiltonian presents time reversal invariance. These points verify

$$\vec{k} = -\vec{k} \mod \vec{G} \tag{2.13}$$

so $\vec{k} = \vec{G}/2$. These are the so called time reversal invariant momenta (TRIM) and verify that Kramer's bands cross in those points and this cross is protected by time reversal invariance. In the other k-points, the Kramer's partner of each eigenvalue is located at $-k$.

The Berry curvature is odd under time reversal

$$\Omega_{\mu\nu}(\vec{k}) = -\Omega_{\mu\nu}(-\vec{k}) \tag{2.14}$$

thus once the Chern number is calculated by its integration, the final result is identically zero. This is because each flux at $\vec{k}$ is compensated by a flux of exactly one flux of opposite sign at $-\vec{k}$. A possible approach to obtain a nonzero result would be to restrict the integration to half of the Brillouin zone to avoid the cancellation. However, in order to have an integer result the parametric space has to be closed so the half zone has to be compacted in some way. Depending on the compactification employed, the Chern number will vary. This is because, given a certain closure, an addition of a sphere will give also a valid closure. The sphere a Chern number equal to 2, so the reduced Chern number is undefined by 2 times the number of additional spheres added, however no matter what compactification is done, the oddness/evenness is well defined. This suggests that time reversal invariance can be classified according to the oddness or evenness of the reduced Chern number which gives a Z_2 topological classification.

Another way to define a topological invariant associated to time reversal systems would be to define something related to the expectation value of the time reversal operator of the form

$$w_{mn}(k) = \langle \Psi_{m,-k} | \Theta | \Psi_{n,k} \rangle \tag{2.15}$$

For the TRIM (which we will denote as Γ_i), the previous matrix is anti-symmetric so its Pfaffian can be defined

$$P(\Gamma_i) = \mathrm{Pf}[w(\Gamma_i)] \tag{2.16}$$

lets remember that the Pfaffian is defined for skew matrices as $\det(A) = [\mathrm{Pf}A]^2$

For each Γ_i a certain number whose value is ± 1 can be defined as the sign of the Pfaffian

$$\delta_i = \frac{\sqrt{\det[(w)(\Gamma_i)]}}{P(\Gamma_i)} \tag{2.17}$$

Each δ_i is gauge dependent, however, the product of all the δ_i is gauge independent and so an invariant of the band structure. So, a topological index ν can be defined as

$$(-1)^{\nu} = \prod_i \delta_i \tag{2.18}$$

so again we obtain that the band structure can be classified in a Z_2 topological class.

For a system which has also inversion symmetry,[27] a matrix analog to w_{mn} can be defined

$$v_{mn}(k) = \langle \Psi_{m,k} | P\Theta | \Psi_{n,k} \rangle \tag{2.19}$$

Defining the expectation value of the parity on the TRIM as $\xi_m(\Gamma_i) = \pm 1$

$$w_{mn} = \xi_m v_{mn} \tag{2.20}$$

and taking into account that having a vanishing Berry curvature one can choose a global gauge where

$$\mathrm{Pf}\ [v(k)] = 1 \tag{2.21}$$

in the whole Brillouin zone so

$$\mathrm{Pf}\ [w]^2 = \det(w) = \det(v) \prod_{n=1}^{2N} \xi_n \tag{2.22}$$

so applying square root

$$\mathrm{Pf}[w] = \mathrm{Pf}[v] \prod_{n=1}^{N} \xi_{2n} \tag{2.23}$$

Thus, the coefficients δ_i can be calculated by the parities at the TRIM by

$$\delta_i = \prod_{n=1}^{N} \xi_{2n}(\Gamma_i) \tag{2.24}$$

In contrast with the general form based on the Pfaffian where a global well defined gauge is needed, with the existence of inversion symmetry the calculation is simplified to calculate the parities of the wavefunctions in the TRIM. This procedure will be the employed in the tight binding calculations and in the DFT calculations to determine the topological ground state of the systems.

2.2 Edge states and the Dirac equation

In this section we will apply the previous concepts to simple toy models to elucidate the strong relation between topologically different vacuums and existence of protected edge states. First we will analyze the two dimensional Dirac equation to begin later to analyze the simplest different models which show protected edge states.

2.2.1 The Dirac equation

A bidimensional representation of the Dirac equation can be easily fulfilled making use of the Pauli matrices

$$H = p_x\sigma_x + p_y\sigma_y + m\sigma_z = \begin{pmatrix} m & p_x + ip_y \\ p_x - ip_y & -m \end{pmatrix} = \begin{pmatrix} m & pe^{i\phi} \\ pe^{-i\phi} & -m \end{pmatrix} \tag{2.25}$$

The eigenvalues of the above equation are $E = \pm\sqrt{m^2 + p^2}$, so for the case $m = 0$ the dispersion relation is linear in p. Applying the concepts of the previous section, one can compute the Berry curvature of the present Hamiltonian. Proceeding first with the case $m = 0$, the eigenfunctions take the form

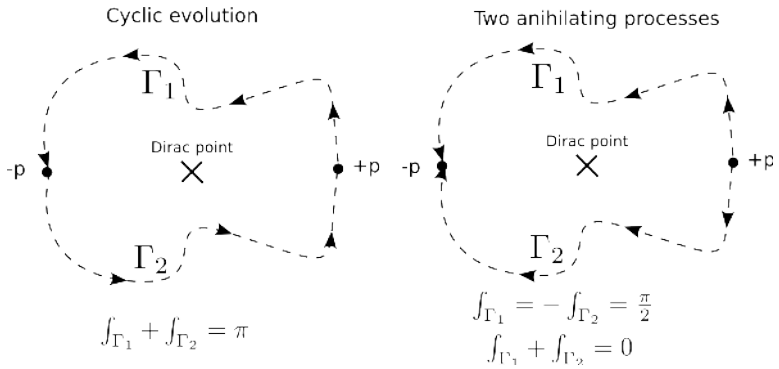

Figure 2.3: Relation between the π Berry phase and the absence of back-scattering in a Dirac equation. the nontrivial phase that the wavefunction gains depending on the path considered makes that each path has an anti-path with opposite amplitude. Since the paths annihilates two by two, the final amplitude for a process of back-scattering is zero.

$$\Psi_\phi = \frac{1}{\sqrt{2}} \begin{pmatrix} 1 \\ e^{-i\phi} \end{pmatrix} \tag{2.26}$$

so the Berry connection and Berry curvature will be

$$A_\phi = \frac{1}{2} \qquad \Omega = 0 \quad \forall \quad p \neq 0 \tag{2.27}$$

In spite of have a vanishing Berry curvature in (almost) all the reciprocal space, the Berry phase of a closed loop than encloses the origin is

$$\oint A_\phi d\phi = \pi \tag{2.28}$$

so the nonvannishing contribution of the Berry curvature comes from a Dirac delta at the origin. The reason of having such a divergence is due to having a touching point between the positive and negative bands.

One important consequence of the π Berry phase is the absence of back-scattering. The reason of such phenomenon is that for each path in a path integral formalism, there is a path that contributes exactly with the opposite amplitude, so when every path is taking into account the probability of suffering a back-scattering event is 0.

To calculate the Berry curvature for $m \neq 0$ it is useful to use another representation of the Berry curvature, changing the differentiation over the

wavefunctions to differentiation over the Hamiltonian. Transforming the terms of the form

$$\langle \partial_\nu n | \partial_\mu n \rangle = \sum_{n'} \langle \partial_\nu n | n' \rangle \langle n' | \partial_\mu n \rangle \tag{2.29}$$

with the relation

$$\langle n | \partial_\mu n' \rangle = \frac{\langle n | \partial_\mu H | n' \rangle}{E_{n'} - E_n} \tag{2.30}$$

the Berry curvature takes the form

$$\Omega_{\mu\nu} = i \sum_{n'} \frac{\langle n | \partial_\mu H | n' \rangle \langle n' | \partial_\nu H | n \rangle}{(E_{n'} - E_n)^2} - (\mu \leftrightarrow \nu) \tag{2.31}$$

Note that the previous form is the integrand of the Kubo formula that arises from second order perturbation theory for the Hall current, so the relation of σ_{xy} with the invariant Chern number is clear.

Taking the eigenfunction of the massive Dirac Hamiltonian for $m > 0$

$$|+\rangle = N \begin{pmatrix} 1 \\ a e^{-i\phi} \end{pmatrix} \qquad |-\rangle = N \begin{pmatrix} -a e^{i\phi} \\ 1 \end{pmatrix} \tag{2.32}$$

$$N = \frac{1}{\sqrt{a^2+1}} \qquad a = \frac{\sqrt{p^2+m^2} - m}{p} \qquad \frac{1-a^2}{1+a^2} = \frac{m}{\sqrt{m^2+p^2}} \tag{2.33}$$

and the derivatives of the Hamiltonian

$$\partial_\phi H = \begin{pmatrix} 0 & ipe^{i\phi} \\ -ipe^{-i\phi} & 0 \end{pmatrix} \qquad \partial_p H = \begin{pmatrix} 0 & e^{i\phi} \\ e^{-i\phi} & 0 \end{pmatrix} \tag{2.34}$$

the Berry curvature of the lowest band takes the form

$$\Omega_{\phi p}^{-,m>0} = \frac{p(1-a^2)(1+a^2)}{2N^4(p^2+m^2)} = \frac{p(1-a^2)}{2(p^2+m^2)(1+a^2)} = \frac{mp}{2(p^2+m^2)^{3/2}} \tag{2.35}$$

For $m < 0$ the calculation is analogous, the only difference is that one has to define the eigenfunctions interchanging the value of the spinors to avoid the singularity of a at $p = 0$. More strictly, it can be checked that the operator $\Sigma = \sigma_x K$ fulfills

$$\Sigma H_m \Sigma^\dagger = H_{-m} \tag{2.36}$$

and since Ω is odd under conjugation it follows

$$\Omega_{\phi p}^{m>0} = -\Omega_{\phi p}^{m<0} \tag{2.37}$$

Note that although for $m = 0$ the curvature vanishes in the whole space for the previous relation, the point $p = 0$ holds a singularity due to the degeneracy of the eigenvalues in that point.

The Chern number can be calculated integrating the Berry curvature in the whole space. Taking the result of Eq. 2.35 the Chern number reads

$$C^{m>0} = \frac{1}{2\pi} \int \frac{mp}{2(p^2 + m^2)^{3/2}} dp d\phi = \frac{1}{2} \tag{2.38}$$

so in general the Chern number of the massive Dirac equation is

$$C = \frac{m}{2|m|} \tag{2.39}$$

It is worth to note that due to do not having a closed parametric space, the Chern number is not an integer. For this fact, when a band structure shows an isolated Dirac point, there has to be another point (or at least a zone with non-vanishing Berry curvature) in other region of the space to compensate the fractional Chern number and obtain an overall integer since the BZ is a closed manifold.

2.2.2 The Jackiw-Rebbi solution

One of the simplest cases of edge states between two different nonequivalent vacuums is the so called Jackiw-Rebbi soliton.[28] The Hamiltonian considered is a one dimensional Dirac equation with a position dependent mass which takes a value $m = +m_0$ in $x = +\infty$ and $m = -m_0$ in $x = -\infty$.

$$H = p_x \sigma_x + m(x)\sigma_z = \begin{pmatrix} m(x) & p_x \\ p_x & -m(x) \end{pmatrix} \tag{2.40}$$

While both asymptotic systems have a mass gap, it will always exist an $E = 0$ bound state in the interface.

$$H|\Psi\rangle = 0 \quad \Rightarrow \quad (-m(x) i\sigma_y + p_x)\,|\Psi\rangle = 0 \tag{2.41}$$

$$\sigma_y|\phi\rangle = |\phi\rangle \quad \Rightarrow \quad \Psi(x) = \phi e^{-\int_0^x m(y)dy} \tag{2.42}$$

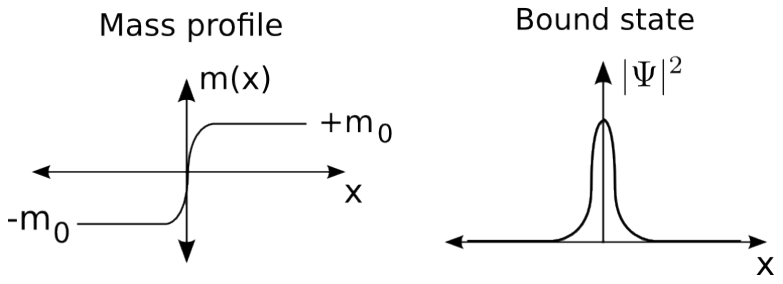

Figure 2.4: Mass profile and solitonic solution of a one dimensional Jackiw-Rebbi model. The gapless kink state is bound to the interface and decays exponentially in the bulk. Also, the existence of the state does not depend on the details of the mass profile in the transition.

From the previous formula it can be checked that the existence of this bound state is due to the change of sign of the mass. As long as the asymptotic masses have a different sign, there will always be a bound state to the interface, so its existence depends on the boundary condition more than on the exact form of the Hamiltonian. One form to understand the previous fact, is to associate an invariant to the Dirac equation of the form $m/|m|$. In this fashion, one can argue that in the boundary of two systems whose Hamiltonian are Dirac equations with different invariants, will have a boundary gapless state. In this sense, the bound state is protected by the topology of the problem and cannot be removed.

The two dimensional analog can be easily constructed. Suppose two regions of the space separated by a one dimensional domain wall. The Hamiltonian will have the form

$$H = p_x\sigma_x + +p_y\sigma_y + m(x)\sigma_z = \begin{pmatrix} m(x) & p_x + ip_y \\ p_x - ip_y & -m(x) \end{pmatrix} \tag{2.43}$$

where $m(x)$ is of the same form as in the one dimensional case. Given that p_y commutes with the Hamiltonian, p_y can be substituted by its eigenvalue k_y. In the particular case of $k_y = 0$, the Hamiltonian is the same as in the one dimensional case, so there will exist also a gapless edge state bounded to the boundary in spite of having two gapped phases.

In fact, the $E = 0$ state is just part of a band that crosses from the negative to positive energies. This can be easily seen taking a particular profile for the mass $m(x) = \lambda x$. Taking the square of the Hamiltonian

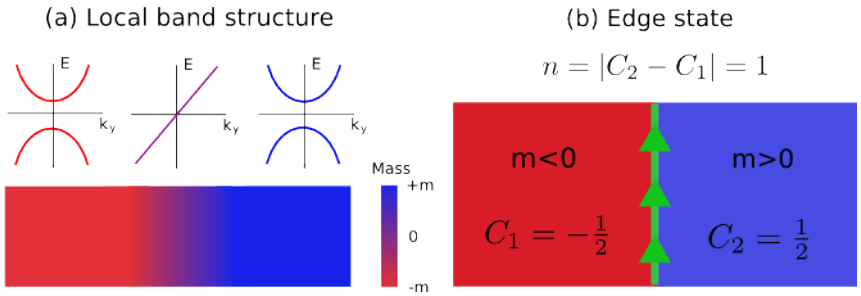

Figure 2.5: (a) Local band structure of a two dimensional Jackiw-Rebbi model and (b) edge state predicted by the index theorem. The present system can be thought as the toy model for more sophisticated models which sustain interface states.

$$H^2 = \begin{pmatrix} \lambda^2 x^2 + p_x^2 + k_y^2 & i\lambda \\ -i\lambda & \lambda^2 y^2 + p_x^2 + k_y^2 \end{pmatrix} \tag{2.44}$$

and taking as basis the harmonic oscillators wavefunctions

$$H^2 = \begin{pmatrix} (2n+1)\lambda + k_y^2 & i\lambda \\ -i\lambda & (2n+1)\lambda + k_y^2 \end{pmatrix} \tag{2.45}$$

gives the eigenvalues

$$E = \pm\sqrt{k_y^2 + 2n\lambda} \tag{2.46}$$

so for the lowest case $n = 0$ the band has the dispersion relation (only one sign survives due to the parity anomaly)

$$E = k_y \tag{2.47}$$

So, the $E = 0$ Jackiw-Rebbi solution would be a state from this band. The fact of having such a ballistic band can be interpreted by the index theorem. This states that in the boundary of two systems there are $C_1 - C_2$ edge states, where C_1 and C_2 are the Chern numbers of the two systems.

2.2.3 The topological Dirac equation

The previous toy model showed that edge states can be associated to the difference of certain invariants of two bulk Hamiltonians. Usual Hamiltonians do not have edge states, so the natural question is if there are some systems

which have irremovable edge states for reasons analogous to the previous one. More precisely, we want to justify the existence of certain edge states as solitonic solutions which interpolate two topologically different systems, the vacuum and the so called topological insulator (TI).

Although the previous model gave a positive answer about the relation of different topological structures and existence of edge state, it is unclear which sign of mass should be related to trivial vacuum and which one to a topological one. To unveil this fact, it is useful to define the following one dimensional modified Dirac equation[17,29] with a mass term dependent on the reciprocal space point

$$H = \begin{pmatrix} m - Bp^2 & p \\ p & -(m - Bp^2) \end{pmatrix} \tag{2.48}$$

Also, it can be easily checked that the eigenvalues of the above equation are

$$E = \pm\sqrt{(m - Bp^2)^2 + p^2} \tag{2.49}$$

so for $m \neq 0$ the spectrum is gapped for every B. The first interesting thing to see is the infrared and ultraviolet limit of the above Hamiltonian. both limits correspond to a Dirac equation but with mass

$$m_{\text{eff}} = m \qquad \text{for} \quad p \to 0 \tag{2.50}$$

$$m_{\text{eff}} = -Bp^2 \qquad \text{for} \quad p \to \pm\infty \tag{2.51}$$

so for $mB > 0$ the chirality of the positive (the same applies for the negative) energy states changes in the reciprocal space. For $mB < 0$, the chirality in the origin is the same as in the infinity. The first one will be denoted as the topological configuration while the second will be the trivial one.

To understand the topological difference of both configurations, we can search for gapless edge states in a seminfinite geometry. For a $E = 0$ localized solution, $p = i\lambda$, and eigenstate of σ_x, $\sigma_x|\Psi\rangle = \chi|\Psi\rangle$,

$$\lambda^2 + \frac{i\chi\lambda}{B} + \frac{m}{B} = 0 \tag{2.52}$$

For an arbitrary boundary condition in $x = 0$, in general one will have a combination of both solutions of the above equation. Given that $\lambda_\pm$ have to have both the same sign of the real part to develop a normalizable solution, it is necessary $m/B > 0$, or in the previous notation $mB > 0$. So, an $E = 0$ edge state solution exists for the topological configuration $mB > 0$ even when the bulk of the system is gapped.

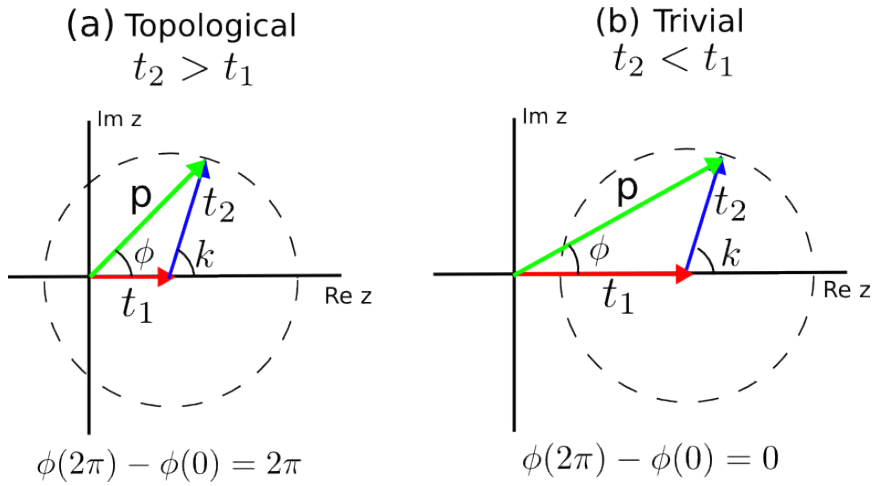

Figure 2.6: Topological (a) and trivial (b) integration path of the Berry phase in the polyacetylene chain. The phase gained in a cyclic evolution takes into account the number of times the phase of the wavefunctions has winded around the origin.

On the contrary to the Jackiw-Rebbi solution, here the topological configuration can be identified unequivocally as the one that develops a gapless edge state in the boundary with a trivial vacuum

2.2.4 Polyacetylene

The simplest case of one dimensional topological insulator is the Polyacetylene chain.[17,30] This system is formed by a one dimensional chain with alternating values of the hopping parameter. When the two hoppings have different magnitude, the system becomes gapped in the bulk. However, depending on the relative strength of the two hoppings, the system can develop topologically protected an edge state in the boundary.

We will consider first an infinite system whose unit cell is a dimer of two atoms of hopping t_1 linked to the neighboring cells by hopping t_2. The Bloch Hamiltonian will be

$$H = \begin{pmatrix} 0 & t_1 + t_2 e^{ik} \\ t_1 + t_2 e^{-ik} & 0 \end{pmatrix} = \begin{pmatrix} 0 & p e^{i\phi} \\ p e^{-i\phi} & 0 \end{pmatrix} \tag{2.53}$$

The eigenvalues are

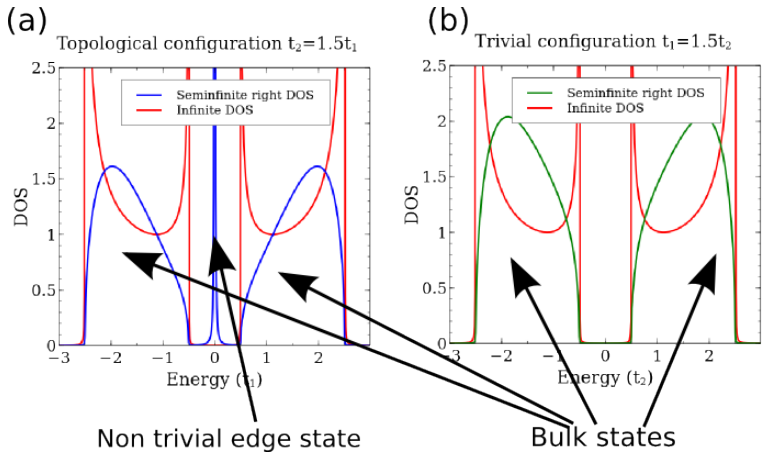

Figure 2.7: Density of states of the edge dimer in the topological (a) and trivial (b) configuration. for the polyacetylene chain. The DOS of the bulk is also shown (red line) to be compared with the edge DOS.

$$E = \pm\sqrt{(t_1 + t_2 \cos k)^2 + t_2^2 \sin^2 k} \tag{2.54}$$

so for $t_1 \neq t_2$ the bulk spectrum is gapped. The eigenfunctions will be

$$|\Psi\rangle = \frac{1}{\sqrt{2}} \begin{pmatrix} 1 \\ e^{-i\phi} \end{pmatrix} \tag{2.55}$$

so the integral of the Berry connection over the full Brillouin zone is

$$\gamma = \oint A dk = i\frac{1}{2}\int_0^{2\pi} e^{i\phi}\partial_k e^{-i\phi} dk = \frac{1}{2}[\phi(2\pi) - \phi(0)] \tag{2.56}$$

In figure 2.6 can be easily seen that

$$\gamma = 0 \quad \text{if} \quad t_2 < t_1 \qquad \text{and} \qquad \gamma = \pi \quad \text{if} \quad t_2 > t_1 \tag{2.57}$$

The existence of an edge state for the topological configuration can be explicitly seen by calculating the density of states (DOS) of a seminfinite chain in both configurations. The DOS can be easily calculated by the edge Green function solving the selfconsistent equation

$$g = \frac{1}{E - H - \Sigma} \tag{2.58}$$

where $\Sigma = t^\dagger g t$ is the usual selfenergy. The bulk DOS can be calculated taking into account that the seminfinite right and left selfenergies have to be added.

In figure 2.7 can be seen that in spite of having a gapped bulk DOS, the topological configuration develops a bound edge state at E=0. This is the topologically protected edge state and is the manifestation of the π Zak phase of the bulk Hamiltonian.

2.3 Graphene

In this section we will review the simplest tight binding models of a honeycomb lattice with an orbital per site. The simplest and most known material whose effective Hamiltonian can be described in this way is the monolayer graphene. However, the interest of these models are far beyond this simple material. The key point is that graphene is the simplest system which presents a honeycomb lattice so it can be treated as a toy model before entering more complex honeycomb systems. The special electronic properties of graphene are just a consequence of the effective Dirac Hamiltonian that arises naturally in a tight binding model.

The symmetries present determine which terms can appear on the effective Hamiltonian, thus restricting the independent parameters that have to be taken into account. For simplicity we will suppose that the point group symmetry is always present, however we will review the cases of both broken and preserved time reversal and inversion symmetry.

2.3.1 Graphene with TR and IS

Graphene presents a honeycomb lattice with carbon atoms in the corner of each hexagon. The simplest model for studying a graphene sheet is to consider the hopping between the p_z orbitals of neighboring atoms in a one particle picture. The whole lattice can be split in two sublattices, the A and B sublattices, in such a way the first neighbors of A atoms are B atoms and vice versa. Due to this connectivity, the simplest unit cell presents two carbon atoms, one from the A lattice and one of the B lattice. In the tight binding picture, the parametric k Hamiltonian to diagonalize will be

$$H(\vec{k}) = \begin{pmatrix} 0 & t(1 + e^{i\vec{k}\cdot\vec{a}_1} + e^{i\vec{k}\cdot\vec{a}_2}) \\ t(1 + e^{-i\vec{k}\cdot\vec{a}_1} + e^{-i\vec{k}\cdot\vec{a}_2}) & 0 \end{pmatrix} \tag{2.59}$$

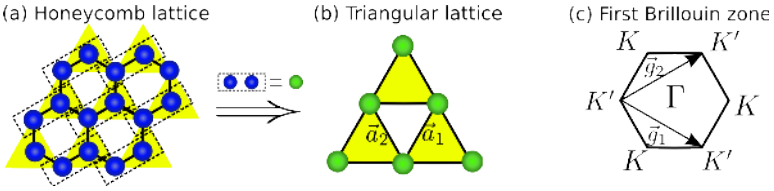

Figure 2.8: (a) Graphene lattice, (b) triangular Bravais lattice and (c) first Brillouin zone of the reciprocal space with the two nonequivalent K and K' points. The effective Dirac equation for the low energy excitations is direct consequence of the bipartite nature of the lattice, so more complex bipartite lattices are likely to show Dirac points in certain regimes. The Dirac points are located in the K and K' points of the Brillouin zone.

There are six k-points in the BZ such that $1 + e^{i\vec{k}\cdot\vec{a}_1} + e^{i\vec{k}\cdot\vec{a}_2} = 0$. Of all those six points, there are only two nonequivalent, being the other four translations by a reciprocal space vector of the first two. In can be easily checked that these special points are in fact the corners of the BZ, and that two nonequivalent points K and K' are related by inversion.

In the neighbor of these points the previous Hamiltonian can be expanded in power series to give a Hamiltonian of the form

$$H(\vec{k}) = \begin{pmatrix} 0 & \hbar v_F(k_x + \tau i k_y) \\ \hbar v_F(k_x - \tau i k_y) & 0 \end{pmatrix} \tag{2.60}$$

where $\tau = 1$ for the K point and $\tau = -1$ for the K' point. Taking natural units $v_F = \hbar = 1$, the previous Hamiltonian is just of the form of a two dimensional Dirac equation, so its eigenvalues are of the form

$$E = \pm\sqrt{k_x^2 + k_y^2} \tag{2.61}$$

The spinorial component of the effective Dirac equation are precisely the components over the A or B sublattice. The fact of having an effective Dirac equation in graphene leads to several well known properties such as its great electrical conductivity (related to the π Berry phase introduced previously) or relativistic Landau levels. The presence of both time reversal and inversion symmetry guarantees that the Chern number is equal to 0. Although each valley has non vanishing Berry phase, they have exactly opposite sign due to the sign dependence of τ.

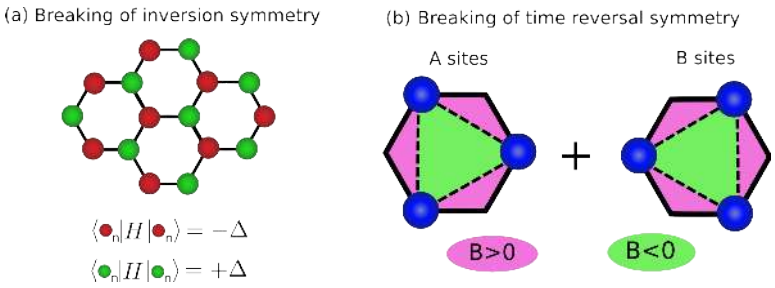

Figure 2.9: (a) Breaking of inversion symmetry and (b) time reversal in the honeycomb lattice. The breaking of IS is fulfilled by a different on-site energy in the A and B atoms. The TR symmetry breaking consists on a magnetic field with zero flux in the unit cell but with negative field in the center and positive near the edges, which is parametrized as an imaginary second neighbor hopping.

2.3.2 Broken inversion symmetry and time reversal: sublattice asymmetry and Haldane model

A possible question in this point is whether a gap can be opened in the effective Dirac equation that arises in graphene. To this point, suppose that somehow a gap has been opened leading to a low energy Hamiltonian of the form

$$H = k_x \sigma_x + \tau k_y \sigma_y + m_\tau \sigma_z \tag{2.62}$$

The existence of spatial inversion symmetry (IS) requires that

$$m_K = -m_{K'} \tag{2.63}$$

On the other hand, time reversal (TR) symmetry requires

$$m_K = m_{K'} \tag{2.64}$$

so for graphene with P and Θ symmetry $m_K = m_{K'} = 0$. The previous argument is valid even in the case of different hoppings in different directions, so the absence of gap is said to be protected by TR and IS. Note that with different hoppings, the Dirac points would not lie exactly in the corners K and K'. So, in the simplified picture worked so far, the only way to open a gap is by breaking either TR or IS.

The simplest way to break IS and preserve TR is by adding a different on-site energy to the A and B atoms. Such a term of this form naturally arises in BN which presents honeycomb lattice with N in the A sites and B sites. In graphene, a term of this form could arise by charge order or by interaction with a substrate. Massive graphene presents a non vanishing Berry curvature. Each valley contributes with a Chern number of $C = \tau \frac{m}{2|m|}$, so the total Chern number is 0 as required by TR.

To break TR but preserve IS, a k dependent term could be added to diagonals of the tight binding Hamiltonian. Such a dependent term naturally arises as a hopping to second neighbors. Breaking of TR requires that this term has to be complex, so it could lead to masses fulfilling $m_K = -m_{K'} \neq 0$. In this case, each valley contributes with the same sign of the Chern number, so the full BZ holds a Chern number C=1. The first neighbors hopping is chosen real as before, so under a loop on the lattice the total phase gained is 0, so there is no net magnetic field in the unit cell. The second neighbor hopping is chosen of the form

$$H_{Hal} = i\lambda_{Hal} \sum_{\langle ij \rangle} (\vec{d_1} \times \vec{d_2}) c_i^\dagger c_j \tag{2.65}$$

where $\vec{d_1}$ and $\vec{d_2}$ are the vectors in the directions of the path to reach the second neighbor.

This model with complex hopping is known as the Haldane model[31] and is known as the first example of quantum Hall effect without magnetic field. It sustains a gapless edge state in each edge due to its Chern number $C = 1$ in accordance with the index theorem, as will be seen below in the TB calculations.

2.3.3 Preserving TR and IS: quantum spin Hall effect in graphene

A question that naturally arises is if there are some kind of system whose transport could be characterized by something like a Chern number, but with time reversal symmetry preserved. The most trivial way of doing this, would be by pasting two Haldane models with conjugated hoppings. In such a system, TR would have not only change the phase of the complex hopping, but also interchanges both subsystems, so global TR would be preserved.

A model like the stated before can be easily fulfilled by including the spin degrees of freedom,[32] in such a way the two subsystems would be the up and down channels, and so TR precisely interchanges up with down.

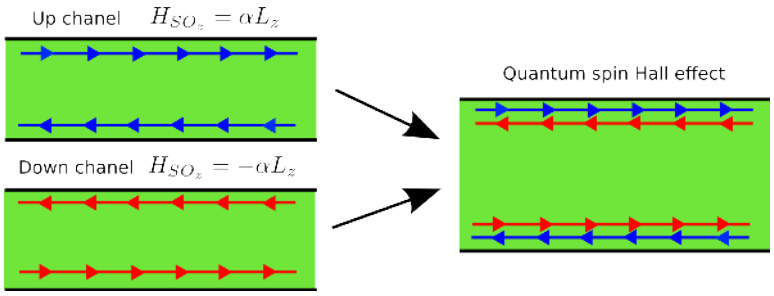

Figure 2.10: The quantum spin Hall effect as two independent Haldane models. Due to the spin conservation of the model, the Kane-Mele model can be discomposed in two Haldane models with imaginary second neighbor hopping with different sign depending on the spin channel. Note that this decomposition has not to be valid for a truly SOC Hamiltonian.

The conjugated second neighbor hopping would be related to a term of the spin-orbit coupling form

$$H_{SO_z} = 2\alpha L_z S_z \tag{2.66}$$

This term would maintain the S_z component of the electrons well defined, but due to the change of sign, each channel would suffer an effective local magnetic field with opposite sign

$$H_{SO_z}|\uparrow\rangle = \alpha L_z|\uparrow\rangle \qquad H_{SO_z}|\downarrow\rangle = -\alpha L_z|\downarrow\rangle \tag{2.67}$$

More exactly, the term that is added to the TB Hamiltonian is

$$H_{SO} = i\lambda_{SO}\sum_{\langle ij\rangle}\vec{S}\cdot(\vec{d}_1\times\vec{d}_2)c_i^\dagger c_j \tag{2.68}$$

The transport of this system would be just the same as in the Haldane model for the different spin channels, in each edge the down spins would move exactly in the opposite direction of the up spins. For each channel, the Chern number would be $|C_{\uparrow,\downarrow}| = 1$, however global TR symmetry requires

$$C = C_\uparrow + C_\downarrow = 0 \tag{2.69}$$

A natural definition would be to define the so called spin Chern number as

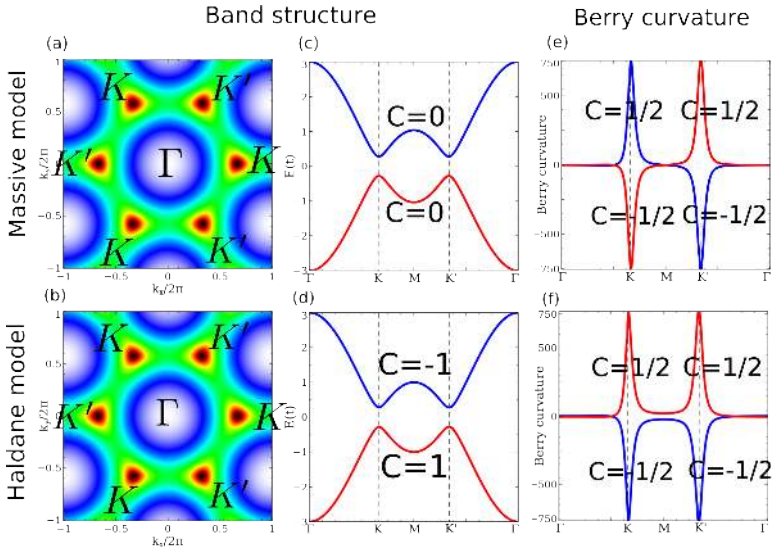

Figure 2.11: (a,b) Two dimensional band structure of the filled band for graphene, (c,d) band structure in certain directions of the BZ and (e,f) Berry curvature in points used in (c,d). (a,c,e) correspond to the massive model whereas (b,d,f) correspond to the Haldane model. The parameters are $\lambda_{Hal} = 0.08$ and $m = 0.28$.

$$C = C_\uparrow - C_\downarrow = 2 \tag{2.70}$$

so in this fashion, the system will be characterized by a quantized spin edge current. However, in more general models beyond graphene the decoupling between the up and down channels is not guaranteed, so the edge modes do not have to be spin polarized but will remain related by time reversal symmetry.

2.3.4 Computational tight-binding model

In the following we will compute the band structure of the tight binding model of graphene by exact diagonalization. The Berry curvature is calculated by finite difference of cyclic Berry connections. A smooth gauge based on choosing a constant component of the spinor in the loop is chosen to avoid numerical instabilities.

We perform calculation for the massive graphene model and for the Haldane model. Both models have in common that in the low energy and

coupling limit the low energy Hamiltonian behaves as two massive Dirac equations. However, since the massive model retains time reversal invariance, the Chern number is identically 0, due to have a mass term with constant sign in both valleys. On the other side, the Haldane model has a mass term which changes sign from one valley to the other (and thus breaks TR invariance), allowing to total Chern number of the filled band $C = 1/2 + 1/2 = 1$.

The existence of a nonvannishing Chern number guarantees the existence of gapless edge states due to the index theorem. Since the massive model has Chern number $C = 0$ it is not guaranteed their existence whereas in the Haldane model we will observe an edge state per boundary of the system.

In figure 2.12 we show the band structure of zigzag ribbons in both models as well as the Berry curvatures obtained. It can be seen that in the massive model there are not gapless edge states (however there are gapped edge states due to the zigzag geometry), whereas in the Haldane model there are gapless edge states both in the weak in the strong and weak limit. Looking at Berry curvatures it is checked that in the massive model different valleys contribute with exactly opposite Berry curvature while in the Haldane model every valley contributes with the same sign.

In the Haldane model, since each edge of the system has only one edge state (required by inversion symmetry), the back-scattering of the edge states is forbidden for wide enough ribbons. For the same reason, small disorder will not lead to localization of the edge sates, however when disorder is strong enough percolation between the two edges by impurity localized bulk states would be possible. The robustness against small disorder of the edge states is responsible for the quantized Hall conductance, and these reasons are the same for the usual quantum Hall effect (both classical or relativistic).

Since the Kane-Mele model can be viewed as two Haldane models with opposite second neighbor coupling, that model will as well support gapless edge states, one for spin up and another for spin down. However due to the TR symmetry of the model, the two channels have to be counter-propagating so the system will not carry net current but will carry a net spin current. Each edge will have an up and down channels propagating in opposite directions.

The edge states of the Kane-Mele model will show robustness for the same reason as in the Haldane model as long as the two channels remain decoupled. To remain decoupled means that in the present model the perturbation Hamiltonian will show time reversal symmetry. If the perturbation is not TR symmetric, the two channels might be mixed and the states can

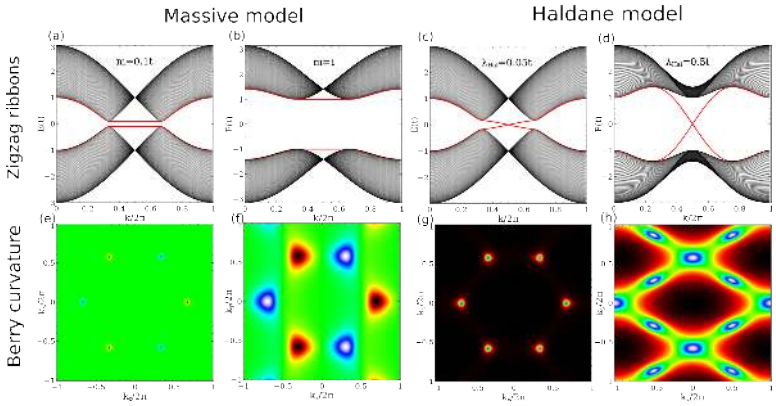

Figure 2.12: Band structure of zigzag ribbons and Berry curvature in the reciprocal space for the massive and Haldane model. It can be seen that the sign of the curvature does not change between valleys in the Haldane and so a nonvanishing Chern number is obtained. In the massive case each contribution in the K valley is canceled by a contribution in the K'.

become localized. Defining the spin current as $J_\uparrow - J_\downarrow$ in the same fashion as the spin Chern number, the robustness of the decoupled edge state will turn the current a quantized quantity.

At this point, the following question is whether systems with Hamiltonians more sophisticated than the Kane-Mele can show a robust edge current. In general, the up and down channels might not be decoupled as in the simple Kane-Mele Hamiltonian, so at first sight it is not clear if the spin current and spin Chern number will remain quantized. The existence of edge states is guaranteed by the calculation of the Z_2 shown in a previous section, but this quantity says nothing about the spin edge current. The result, which will not be calculated here is that a generalized formulation of the spin Chern number[21] which remains quantized can be performed. However, the spin current will not be quantized,[12,14] since the edge states do not have to be spin filtered in general, but will be robust.[22]

Chapter 3

The perovskite bilayer

3.1 Introduction

The perovskite structure, shown in Fig 3.4, with notation ABO_3, consists of a cubic lattice of B atoms surrounded by an octahedral environment of O atoms and with an A atom in the middle of the cube. The O atoms are located in the middle of the B-B distances.

In our particular case, we will choose the A and B atoms such that their roles can be thought in the following way. The A atoms are not electronically relevant given that they loose all their valence electrons whereas the B atoms loose a certain number of valence electrons until the oxygen reaches -2 state. The rest of the electrons of the B atoms will lie in the d-shell, perturbed by the octahedral field created by the oxygen atoms. In addition to this perturbation, the oxygen atoms will let hopping between neighboring B atoms via virtual processes. Also, many body couplings between neighbors via the oxygen may create a Heisenberg term which will be responsible of magnetism.

A honeycomb structure can be constructed from a perovskite unit cell as can be seen in Fig. 3.2, where a perovskite bilayer grown along the (111) direction made of an open-shell oxide is sandwiched by an isostructural band insulating oxide. The metal atoms of the bilayer form the honeycomb lattice. It has been shown that (111) multilayers can develop topological phases,[26,36–39] as well as spin liquid phases and non-trivial superconducting states.[40] Topological insulating phases have been predicted for various fillings of the d shell,[26] here we will focus on the large SOC limit (5d electrons) and formal d^5 filling. We will study two different multilayers, $(SrTiO_3)_7/(SrIrO_3)_2$ and $(KTaO_3)_7/(KPtO_3)_2$ and we will focus on the re-

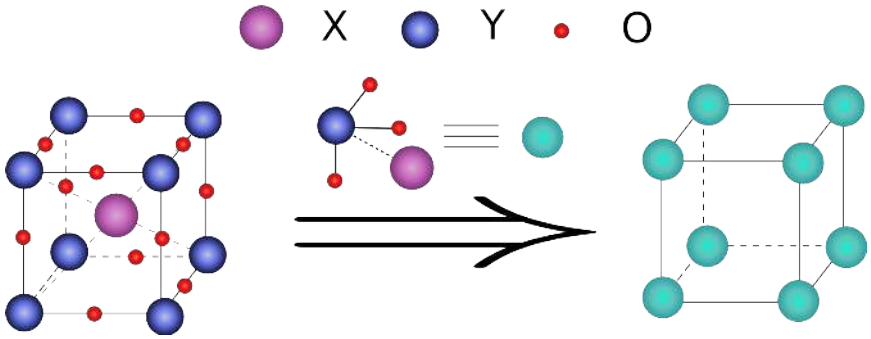

Figure 3.1: Scheme of the cubic perovskite structure XYO_3.

alization of a nontrivial $\nu = 1$ ground state. $SrIrO_3$ ($a_{SrIrO_3} = 3.94\mathring{A}$)[41] is a correlated metal[42] whose lattice match with $SrTiO_3$ (STO) would be close enough ($a_{SrTiO_3} = 3.905\mathring{A}$)[43] for them to grow epitaxially with standard growth techniques. $KPtO_3$ has not been synthesized (to the best of our knowledge) but our calculations ($a_{KPtO_3} = 4.02\mathring{A}$) show a reasonable lattice match with $KTaO_3$ would be possible ($a_{KTaO_3} = 3.98\mathring{A}$[44]). The first multilayer is an iridate very similar to the well known Na_2IrO_3.[45,50] This last system presents a honeycomb lattice of Ir atoms at t_{2g}^5 filling and is predicted to develop the QSHE, however electron correlation would develop an antiferromagnetic order in the edges. We will study the dependence of the topological ground state on the applied uniaxial strain and the electron-electron interaction and we will determine a transition between two topological phases in both materials. The work is organized as follows. Firstly, we introduce a simple tight binding (TB) model as in[26] focusing on the t_{2g}^5 case. In Section III we use density functional theory (DFT) calculations to study the evolution of both multilayers with uniaxial strain and on-site Coulomb repulsion and we determine the ground state of each material. In Section IV we study the stability of the topological phase against TR and IS breaking using both TB and DFT calculations. Finally in Section V we summarize the results obtained.

3.2 Tight binding model

In this section we explain the form of the different terms of the TB Hamiltonian

$$H = H_{SO} + H_t + H_{tri} + H_m \tag{3.1}$$

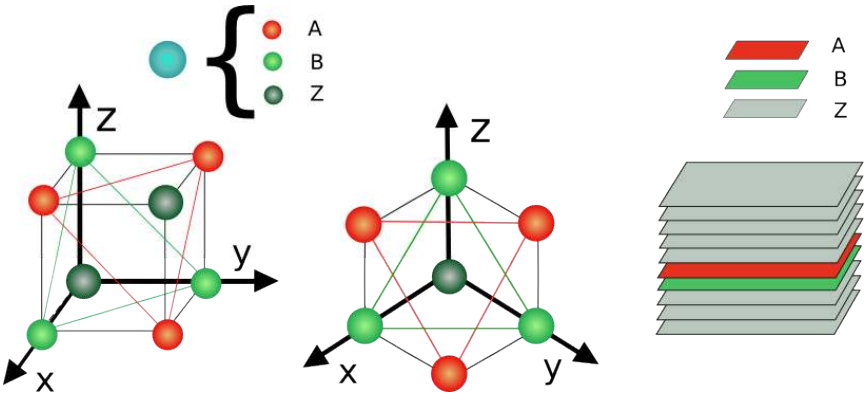

Figure 3.2: Construction of the bilayer and scheme of the multilayer considered in the DFT calculations. The TM atoms are arranged in a triangular A and B lattice in the (111) direction in such a way the two will form a buckled honeycomb lattice. The Z atom corresponds to the insulating layer (in our case $SrTiO_3$ or $KTaO_3$) and does not participate in the honeycomb.

3.2.1 Spin-orbit term

We want to obtain the form of the SOC restricted to the t_{2g} subspace. Taking the basis

$$|yz\rangle = \begin{pmatrix}1\\0\\0\end{pmatrix} \quad |xz\rangle = \begin{pmatrix}0\\1\\0\end{pmatrix} \quad |xy\rangle = \begin{pmatrix}0\\0\\1\end{pmatrix} \tag{3.2}$$

can be easily seen that the representation $L_i = \hbar l_i$ takes the form

$$l_x = \begin{pmatrix}0 & 0 & 0\\0 & 0 & i\\0 & -i & 0\end{pmatrix} \quad l_y = \begin{pmatrix}0 & 0 & i\\0 & 0 & 0\\-i & 0 & 0\end{pmatrix} \tag{3.3}$$

$$l_z = \begin{pmatrix}0 & i & 0\\-i & 0 & 0\\0 & 0 & 0\end{pmatrix}$$

The SOC term has the usual form

$$H_{SO} = \frac{2\alpha}{\hbar^2}\vec{L}\cdot\vec{S} = \alpha\vec{l}\cdot\vec{\sigma} \tag{3.4}$$

where σ_i are the usual Pauli matrices acting on spin space. The representation follows the commutation relation $[l_i, l_j] = -i\epsilon_{ijk}l_k$ so defining

$J_i = S_i - L_i$ the usual commutation relations hold. This change of sign introduces an overall minus sign on the eigenvalues so the spectrum results in a $j = 3/2$ quadruplet with $E_{j=3/2} = -\alpha$ and $j = 1/2$ doublet with $E_{j=1/2} = 2\alpha$.

3.2.2 Hopping term

Each site has three bonds directed along the edges of the perovskite structure. The bonds link the A and B sublattices so there will be three different overlaps $t_i = \langle A|H_t|B\rangle$ depending on the direction

$$(t_x, t_y, t_z) = t(\tau_x, \tau_y, \tau_z) \tag{3.5}$$

The hopping takes place through the overlap of the t_{2g} orbitals of the TM and the oxygen p orbitals, It can be easily checked that the main contribution gives a matrix form that can be casted in the form

$$(\tau_x, \tau_y, \tau_z) = (l_x^2, l_y^2, l_z^2) \tag{3.6}$$

3.2.3 Trigonal term

Due to the geometry of the system, a possible term in the Hamiltonian that does not break the spatial symmetries of the system is a trigonal term. This term will differentiate the perpendicular direction from the in-plane directions. This term will behave as an on-site term which mixes the t_{2g} states without breaking the symmetry between them so the general form in the t_{2g} basis is

$$H_{tri} = \lambda_{tri} \begin{pmatrix} 0 & 1 & 1 \\ 1 & 0 & 1 \\ 1 & 1 & 0 \end{pmatrix} \tag{3.7}$$

3.2.4 Mass term

A term which makes the two sublattices nonequivalent will break inversion symmetry. The minimal term which fulfills this is

$$H_m = m s_z = m \begin{pmatrix} I_A & 0 \\ 0 & -I_B \end{pmatrix} \tag{3.8}$$

where I_A and I_B are the identity matrix over the A and B sublattices

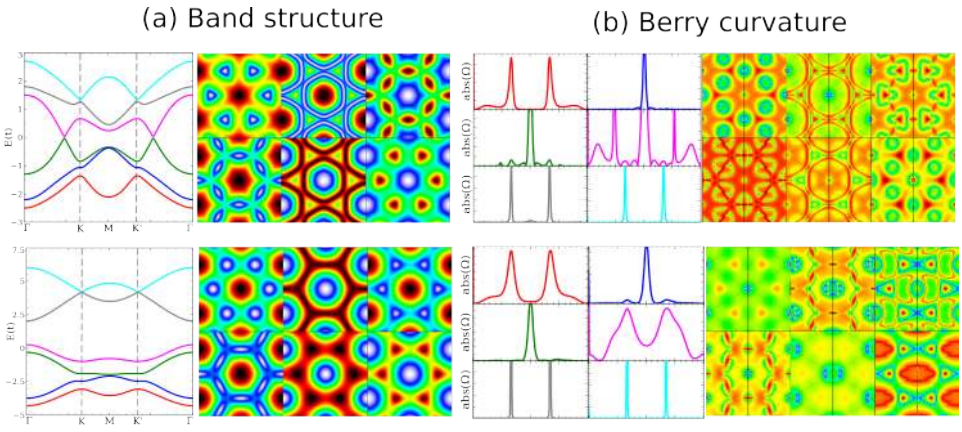

Figure 3.3: Band structure and absolute Berry curvature of the tight binding model. The parameters are $\lambda_{SO} = 0.2t$, $\lambda_{tri} = 0.3t$ for the first row and $\lambda_{SO} = 2t$, $\lambda_{tri} = 0.3t$ for the second row.

3.2.5 Appearance of the model

First we will calculate the band structure in the regimen of weak and strong orbit coupling. Since we would like to preserve both time reversal and inversion symmetry, applying the same argument as the one of the Kramer's degeneracy to the operator $P\Theta$, in each k-point we will have degeneracy two. This fact arises a new problem which is that in this case we have also U(2) symmetry in the reciprocal space apart from the usual U(1). To do a strict calculation, we should compute the non abelian Berry curvature instead the usual abelian one. However, due to the random matrix problem there will be numerical instabilities when the different components of the gauge field are calculated. To avoid this problem, we have chosen to break the U(2) symmetry to the usual U(1) by a sublattice asymmetry which breaks inversion symmetry. Since the meaning of the Berry curvature in the regularized problem is not clear, the calculation will only lead us to identify the topologically interesting points of the band structure. Since we could also have broken the U(2) symmetry by a ferromagnetic or antiferromagnetic field to regularize the calculation, it is more suggestive to preserve time reversal symmetry even if the breaking was present only as an anomaly.

In figure 3.3 the band structure is shown and the absolute value of the Berry curvature in the regularized system. It is clearly seen that the upper two bands develop a Dirac point in the k-point as in graphene. In the

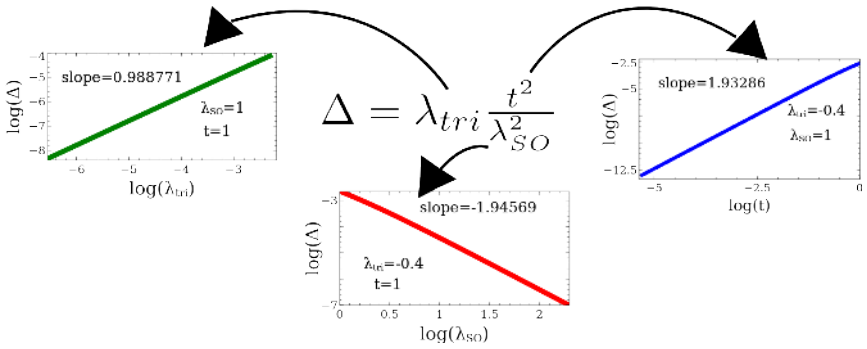

Figure 3.4: Evolution of the gap with the different parameters of the system and perturbation term which will lead to such behavior.

following we will see precisely that the perovskite at t_{2g}^5 behaves very similar to graphene, which will be the behavior expected from the band structures and Berry curvatures shown.

3.2.6 Full Hamiltonian

The octahedral environment of oxygen surrounding the transition metal atoms decouple the d levels in a t_{2g} sextuplet and an e_g quadruplet. Given that the crystal field gap is higher than the other parameters considered we will retain only the t_{2g} levels. The Hamiltonian considered for the t_{2g} levels takes the form

$$H = H_{SO} + H_t + H_{tri} + H_m \tag{3.9}$$

H_{SO} is the SOC term, which gives rise to an effective angular momentum $J_{eff} = S - L$ which decouples the t_{2g} levels into a filled j=3/2 quadruplet and a half filled $j = 1/2$ doublet. H_t is the hopping between neighboring atoms via oxygen that couples the local orbitals without mixing j_z. H_{tri} is a local trigonal term which is responsible for opening a gap (as we will see below) without breaking TR and IS. H_m is a term which breaks IS making the two sublattices nonequivalent tending to open a trivial gap by decoupling them. In the following discussion we will suppose that this last term is zero, but we will analyze its role in section IV.

We are interested in two different regimes as a function of SOC strength: strong and intermediate. We call strong SOC to the regime where the j=3/2 and j=1/2 are completely decoupled so that there is a trivial gap between

them. We will refer to an intermediate regime if the two subsets are coupled by the hopping. The key point to understand the topological character of the calculations is that a t_{2g}^5 configuration can be adiabatically connected from the strong to the intermediate regime without closing the gap. The argument is the following, beginning in the strong SOC regime it is expected that a four band effective model will be a good approximation. In this regime the mathematical structure of the effective Hamiltonian turns out to be equivalent to graphene. The trigonal term is responsible for opening a gap Δ via a third order process in perturbation theory

$$\Delta \sim \lambda_{tri} \frac{t^2}{\alpha^2} \tag{3.10}$$

where λ_{tri} is the trigonal coupling t is the hopping strength and α the SOC parameter. It can be checked by symmetry considerations that the restriction of the matrix representations leads to this term as the first non-vanishing contribution in perturbation theory. Eq. (2) has been checked by a logarithmic fitting of numerical calculations of the full model. This term will open a gap in the K point conserving TR and IS and thus realizing a $\nu = 1$ ground state.[27]

As SOC decreases, the gap becomes larger while the system evolves from the strong to the intermediate regime, so the intermediate regime is expected to be a topological configuration[26] with a non-vanishing gap. Note that even though perturbation theory will only hold in the strong regime, the increase in the gap as the system goes to the intermediate regime suggests that the t_{2g}^5 configuration will always remain gapped. This argument is checked by the numerical calculations shown below.

3.2.7 Results from tight binding calculations

In Fig. 3.5 we show the results of a calculation using the TB Hamiltonian proposed above. Figure 3.5a is the bulk band structure for strong and intermediate SOC strength α. If a non-vanishing trigonal term is included, it opens a gap in the Dirac points of the band structure generating topologically non-trivial configurations. We can see this clearly in Fig. 3.5b, where the band structure close to the Fermi level in the vicinity of the K point is shown.

The topological character of each configuration is defined by the ν topological invariant which for a band in an IS Hamiltonian can be calculated as[27]

$$(-1)^{\nu_b} = \prod_{\text{TRIM}} \langle \Psi_b | P | \Psi_b \rangle \tag{3.11}$$

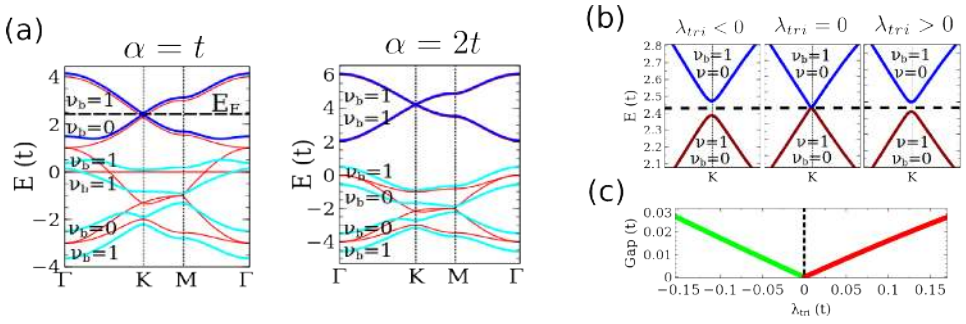

Figure 3.5: (a) Band structure of the TB model with intermediate $\alpha = t$ (left) and strong $\alpha = 2t$ (right) SOC strength and $\lambda_{tri} = -0.5$, the difference between the two cases relies on the ν_b invariant of last filled band. The red lines are the band structure with $\lambda_{tri} = 0$ (b) Band structure zoomed for the j=1/2 bands near the K point for negative ($\lambda_{tri} = -0.5$), zero and positive ($\lambda_{tri} = -0.5$) (c) Evolution of the gap in the K point with λ_{tri} for the intermediate regime.

where the product runs over the four time reversal invariant momenta (TRIM). The full invariant of a configuration will be the product of the last equation over all the occupied bands

$$\nu = \sum_{\text{occ.bands}} \nu_b \ (\text{mod } 2) \tag{3.12}$$

For a t_{2g}^5 filling the first unfilled band has always $\nu_b = 1$ but the difference between strong and intermediate SOC is the ν_b invariant of the last filled band. For strong SOC the j=1/2 and j=3/2 are completely decoupled so a t_{2g}^4 configuration would be topologically trivial, being the invariant of the fifth band $\nu_b = 1$. However, when SOC is not sizable the bandwidths are large enough to couple the j=1/2 and j=3/2 levels so that the t_{2g}^4 filling is a topological configuration. In both cases the t_{2g}^5 is topologically non-trivial. We will see below using DFT calculations that the systems under study (TMO's with 5d electrons in a perovskite bilayer structure) are in this intermediate SOC regime.

Figure 3.5b shows the bulk band structure, focusing now in the j=1/2 bands, for negative, zero and positive trigonal terms. The number ν_b is the invariant of the band while ν is the sum of the invariants of that band and the bands below it. No matter what the sign of λ_{tri} is, the configuration becomes non-trivial, being its role to open a gap in the K point around the

Fermi level. In the DFT calculations below, it will be seen that a change of sign of the trigonal term can be understood as a topological transition between a low U topological insulating phase (LUTI) and a high U topological insulator (HUTI), across a boundary where the system behaves as a topological semimetal (TSM).

3.3 DFT calculations

3.3.1 Computational procedures

Ab initio electronic structure calculations have been performed using the all-electron full potential code WIEN2K[53] The unit cell chosen is shown in Fig. 3.2. It consists of 9 perovskite layers grown along the (111) direction, 2 layers of $SrIrO_3$ ($KPtO_3$) which conform the honeycomb and 7 layers of $SrTiO_3$ ($KTaO_3$) which isolate one honeycomb from the other.

For the different off-plane lattice parameters along the 111 direction of the perovskite considered, the structure was relaxed using the full symmetry of the original cell. The exchange-correlation term is calculated depending on the case using the generalized gradient approximation (GGA) in the Perdew-Burke-Ernzerhof[54] scheme, local density approximation+U (LDA+U) in the so-called "fully located limit"[55] and the Tran-Blaha modified Becke-Jonsson (TB-mBJ) potential.[56]

The calculations were performed with a k-mesh of 7 × 7 ×1, a value of $R_{mt}K_{max}$= 7.0. SOC was introduced in a second variational manner using the scalar relativistic approximation.[57] The R_{mt} values used were in a.u. 1.89 for Ti, 1.91 for Ir, 2.5 for Sr and 1.67 for O in the Ir-based multilayer and 1.93 for Ta, 1.92 for Pt, 2.5 for K, 1.7 for O in the Pt-based multilayer.

3.3.2 Band structure of the non-magnetic ground state

The systems chosen to study a d^5 filling in a honeycomb lattice with substantial SOC are the multilayers $(SrTiO_3)_7/(SrIrO_3)_2$ and $(KTaO_3)_7/(KPtO_3)_2$ formed by perovskites grown along the (111) direction.

First the structure is optimized for different lattice parameters c respecting IS using GGA and without SOC. This means that mainly only the interplanar distances in the multilayers are relaxed. For the energy minimum the band structure is calculated turning on SOC.

The band structure using three exchange-correlation schemes (GGA, LDA+U and TB-mBJ) develops the same structure. The ν_b topological invariant of each band is calculated as in the TB model,[27] the topological

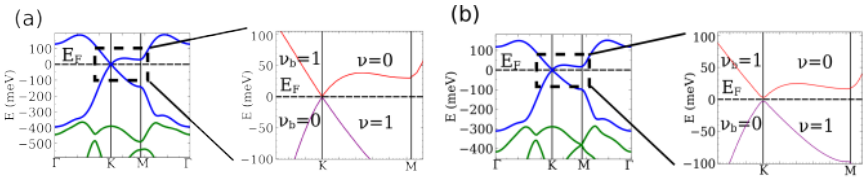

Figure 3.6: Band structure obtained in the DFT calculations for the optimized lattice parameter c. The calculations were performed with TB-mBJ for both $(SrTiO_3)_7/(SrIrO_3)_2$ (a) and $(KTaO_3)_7/(KPtO_3)_2$ (b). The right panels are the band structure near the Fermi level with the topological invariants displayed.

invariant being the sum of the ν invariants over all the occupied bands. Figure 3.6 shows the band structure calculated with TB-mBJ as well as the ν_b invariants also obtained ab initio. The difference in the curvature of the bands with respect to the result obtained with the TB model is due to the existence of bands near the bottom of the j=3/2 t_{2g} quadruplet which are not considered in the TB Hamiltonian. Each band has double degeneracy due to the combination of TR and IS. At the optimized c, the gap between the last filled and the first unfilled band is located at the corner of the Brillouin zone (K-point). At low c (unstable energetically but attainable via uniaxial compression), GGA predicts that the system can become a metal by closing an indirect gap between the K and M points, however TB-mBJ calculations predict that a direct gap is localized at the K point. For all the calculations the ground state has $\nu = 1$ and thus it develops a topological phase. The last filled band turns out to have $\nu_b = 0$ so by comparison with the TB results the system corresponds to the intermediate SOC limit. If a 5d electron system like this is in the intermediate SOC limit, it is hard to imagine how one can build a TMO heterostructe closer to the strong SOC limit. The first unfilled band has $\nu_b = 1$ as expected since a t_{2g}^6 configuration will be a trivial insulator with a gap opened by the octahedral crystal field.

The way a trigonal field is present in the DFT calculations is mainly in two ways. On one hand, strain along the z direction varies the angles of the cubic perovskite leading to a mixing term between the t_{2g} levels. We define this deformation as $\epsilon_{zz} = \frac{c-c_0}{c_0}$ where c_0 is the off-plane lattice constant with lowest energy. On the other hand, an on-site Coulomb repulsion defined on the TM by using the LDA+U method has precisely the symmetry of the bilayer, i.e. trigonal symmetry, so varying in some way the on-site potential

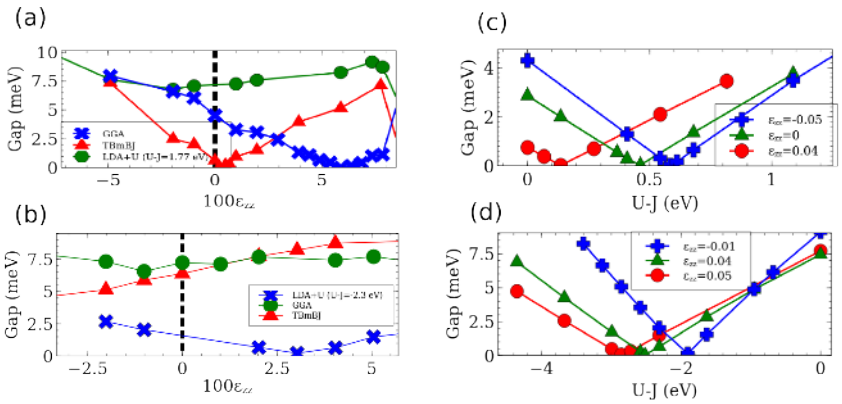

Figure 3.7: Evolution of the gap as a function of the uniaxial strain for the Ir-based multilayer (a) and Pt-based multilayer (b). Evolution of the gap with the on-site interaction for the Ir-based multilayer (c) and Pt-based multilayer (d). It is seen that both systems develop the same behavior although at different U's.

(always preserving parity symmetry) will have the effect of a trigonal term in the Hamiltonian.

According to this, it is expected that in a certain regime, variations in ϵ_{zz} can be compensated by tuning U. In this regime, similar to what we discussed above, the system will develop a transition between two topological phases: a LUTI and a HUTI. At even higher U the system will show magnetic order, however we will address this point later and by now we will focus first on the non-magnetic (NM) phase. In order to study the phase diagram defined by the parameters ϵ_{zz} and U, we will perform calculations keeping one of them constant and determine how the gap closes, keeping track of the parities at both sides of the transition.

3.3.3 Evolution of the gap with uniaxial strain

Here we will discuss the behavior of the gap in the K point with ϵ_{zz} keeping U and J constant. First we analyze the behavior of both materials in parameter space showing their similarities finishing characterizing the actual position of the ground state of the system in the general phase diagram.

First we focus on the $(SrTiO_3)_7/(SrIrO_3)_2$ case. As shown in Figure 3.7, the gap closes as a function of c, so uniaxial strain can drive the system

between two insulating phases just as λ_{tri} does in our TB model. However, for high U the transition point disappears. For low U, ϵ_{zz} can drive the system from a positive trigonal term to a negative one. This means that uniaxial strain can change the sign of the effective trigonal term of the Hamiltonian. However, for high U, strain is not capable of changing the trigonal field, so the system remains in the same topological phase for every ϵ_{zz}. For the calculations using the TB-mBJ scheme, the transition point takes place almost at $\epsilon_{zz} = 0$.

Now we will focus on the $(KTaO_3)_7/(KPtO_3)_2$ system. For the GGA calculations the transition with ϵ_{zz} disappears, being the system always in the HUTI phase. If the system is calculated using LDA+U with U negative, the behavior is similar to the previous system and the transition point of TSM reappears. Thus, the present system (Pt-based), though isoelectronic and isostructural, can be understood as the strong-U limit of the previous system (Ir-based). The band gap is larger, which is a sought-after feature of these TI, but not large enough to make it suitable for room temperature applications.

3.3.4 Evolution of the gap with U at constant ϵ_{zz}

The Hamiltonian felt by the electrons depends also on the on-site Coulomb interaction between them. If the variation in the term of the Hamiltonian that controls it takes place only in the TM atoms, the symmetry of the varying term will have the same local symmetry as the TM atoms, i.e. trigonal symmetry. Thus, it is expected that a variation in U will have a similar effect as λ_{tri} in the TB model, so the gap can also be tuned by the on-site interaction.

Figure 3.7 shows the behavior of the gap for both systems in an LDA+U scheme with J=0.95 eV as the parameter U is varied.

The slow increase of the gap with U suggests that the gap opened is not that of a usual Mott insulator and reminds rather to the slow increase obtained in the TB model. In fact, calculation of the ν invariant shows again a topological phase on both sides of the transition.

Both systems develop a transition between the LUTI at low U to the HUTI phase at high U. However, the transition point of $(SrTiO_3)_7/(SrIrO_3)_2$ is at positive U's, for the $(KTaO_3)_7/(KPtO_3)_2$ the transition appears at negative U's, so for all possible reasonable U values the system will be a HUTI.

For $(SrTiO_3)_7/(SrIrO_3)_2$ it is possible to use this transition to estimate which value of U should be used in an LDA+U calculation for these 5d

systems to reproduce the result of the TB-mBJ calculation. This is often a matter of contention when dealing with insulating oxides containing 5d TM's.[45,58] TB-mBJ calculations have proven to give accurate results of band gaps in various systems,[61] however in strongly correlated d systems the results of the functional are not a great improvement of the usual GGA scheme.[62] On the other hand, it has been shown in the past (for 3d electron systems) that a TB-mBJ calculation can be compared with an LDA+U calculation for a U value that matches nicely spectroscopy data, lattice parameters and density of states.[63] Either way, due to the relatively low U of Pt and Ir compounds in comparison with other TM, we will in principle accept this scheme and, in order to estimate an approximately correct value of U to use in an equivalent LDA+U calculation, one possible route is to look for which is the value that reproduces the same transition point as the TB-mBJ calculation. From Fig. 3.7c it can be checked that the gap closes at U-J=0.45 eV being this value in agreement with the ones suggested in some references.[45,46] This approach suggests that the values which might be used in an LDA+U calculation to mimic the TB-mBJ result are on the order of $U = 1.4$ eV and $J = 0.95$ eV. On the other hand, other works relate to value of U on the order of 2 eV,[47,48] however due to the well known property dependence of the value of U,[49] it is still unclear which is the correct value to study these topological phases. Therefore, our result can serve as a reference for other ab initio based phase diagrams for iridates where topological phases have been predicted as a function of U.[58] Moreover, we study this system in a broad range of U values and using different exchange-correlation schemes to provide a broad picture of the problem.

Recently topological phases dominated by interactions, called topological Mott insulating phases, have been theoretically found,[51,52] being this term employed for physically different phenomenon. In the HUTI phase, the gap of the systems is enhanced by increasing U parameter so that the system might be robust against electron-electron interactions. In the same fashion a usual band insulator can be connected to a Mott insulating phase,[59,60] the previous robustness suggests that the HUTI phase might be adiabatically connected to an integer Mott insulating phase. Whether this is an artifact of the DFT method or an acceptable mean field approach of a many body problem is something that can only be clarified with experiments.

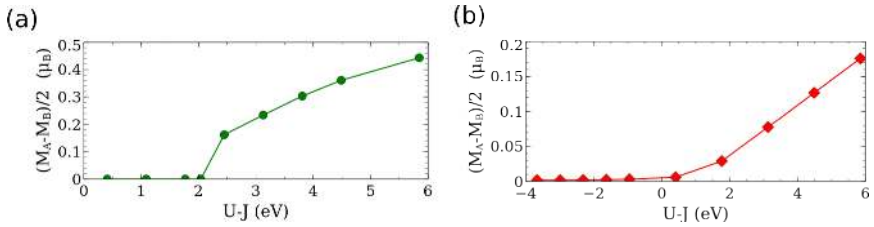

Figure 3.8: Difference of the sublattice magnetization for the $(SrTiO_3)_7/(SrIrO_3)_2$ (a) and $(KTaO_3)_7/(KPtO_3)_2$ (b). At high U the systems develop an AF order, however at realistic U's both systems remain non-magnetic.

3.4 Stability of the topological phase

So far we have considered a system with both TR and IS. However, given that the Z_2 classification is valid only for TR systems it is necessary to determine if the ground state possesses this symmetry. IS breaking could destroy the topological phase opening a trivial gap by decoupling both sublattices. TR symmetry breaking will be fulfilled by a magnetic ground state whereas IS breaking will be realized by a structural instability. In this Section we will study the two possibilities and conclude that both systems remain in the topological state in their ground states.

3.4.1 Stability of time reversal symmetry

Increasing electronic interactions will drive the NM ground state to a magnetic trivial Mott insulating phase at very high U. For a magnetic d^5:S=1/2 localized-electron system, from Goodenough's rules[64] an antiferromagnetic (AF) exchange between the two sublattices is expected which would create an AF ground state breaking both TR and IS. To check this result, we have performed DFT calculations within an LDA+U scheme taking J=0.95 eV and varying U.

For both systems the calculations have been carried out at different U's for the NM and AF configurations. In both cases the ground state is AF at high U. Also, the sublattice magnetization increases with U. The main difference is that in $(SrTiO_3)_7/(SrIrO_3)_2$ a NM phase can be stabilized even at high U in spite of being the AF phase lower in energy. In contrast, in $(KTaO_3)_7/(KPtO_3)_2$ it has not been possible to stabilize a NM phase. Figures 3.8a and 3.8b show the evolution of the sublattice magnetic moment

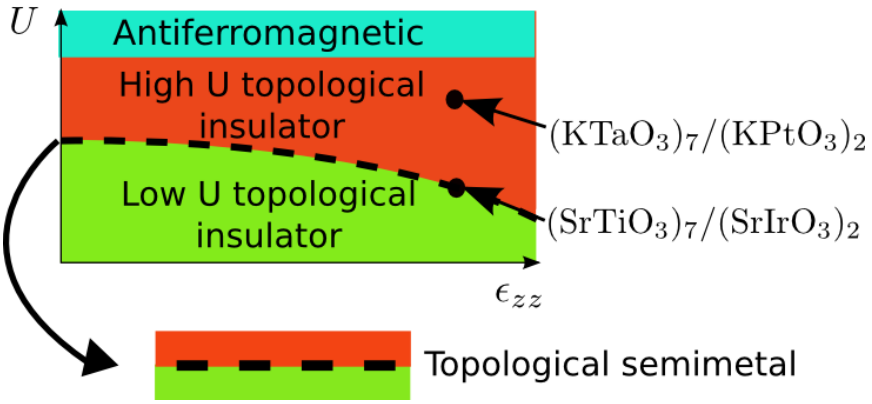

Figure 3.9: Phase diagram in ϵ_{zz}-U space, the approximate position of the ground state of both systems is indicated.

for both compounds.

Also, a ferromagnetic (FM) phase has been analyzed, being the least preferred one. In the Ir compound a FM phase can be stabilized but has always higher energy than the NM or AF. In the Pt compound a FM phase cannot be stabilized like in the case of NM calculations. The true ground state of the system would be a TI phase in the Pt-based multilayer (or TSM in the Ir-based multilayer) depending on the value of U employed, so if the correct value to be used is larger than the critical value, the topological Z_2 phase will break down and the edge states would become gapped. Thus the experimental measurement of the magnetic moment of the ground state, of these bilayers would shed light into the correct value of U which should be used in these and other similar compounds. To summarize, the system shows a NM ground state for both compounds until a certain U (larger than the value of U that would be equivalent to TB-mBJ calculations) where the system becomes AF (see Fig. 3.9).

3.4.2 Stability of inversion symmetry

The topological properties of this system rely on both TR and IS. Tight-binding calculations predicted that non-invariant parity terms with energy associated of the order of magnitude of the topological gap could eventually drive the topological phase to a trivial one.

First we will discuss the $(SrTiO_3)_7/(SrIrO_3)_2$ system. The simplest IS breaking could be driven by a structural instability. To study the structural

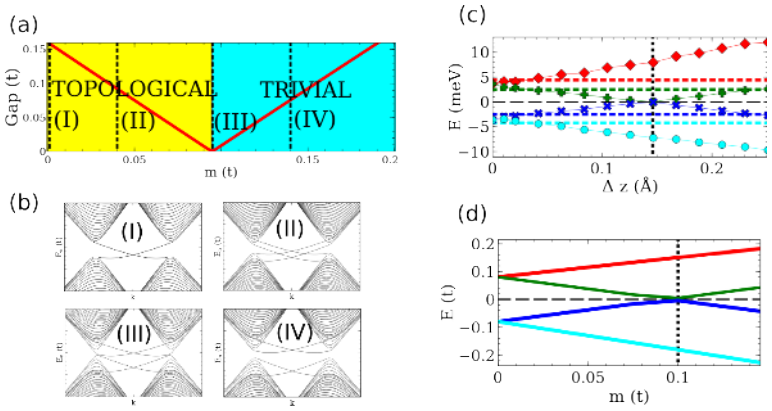

Figure 3.10: (a) Evolution of the gap in the TB model as a function of m, the closing point spots the transition between topological and trivial phase. (b) Bands of zigzag ribbons at different m, for low there are gapless edge states while for large m the edge states become gapped. (c) Evolution of the eigenvalues obtained in the DFT calculation of $(KTaO_3)_7/(KPtO_3)_2$, the dashed lines correspond to the fully relaxed structure. (d) Evolution of the four eigenvalues closest to the Fermi level for the TB model.

stability of the structure, we have displaced one of the TM atoms from its symmetric position and then relaxed the structure. As a result, the structure returned to the symmetric configuration. However, due to being in the transition point between the two topological phases any external perturbation (such as a perpendicular electric field) could break inversion symmetry. This system would be classified more as a topological semimetal rather than a topological insulator due to the (almost) vanishing gap of the relaxed structure.

Now we will proceed to $(KTaO_3)_7/(KPtO_3)_2$. The first difference between this and the previous system is that in the present case the structure is well immersed in the HUTI. A large IS breaking is expected to drive the system to a trivial phase where the sublattices A and B would be decoupled. However, to change its topological class, the system has to cross a critical point where the gap vanishes in some point of the Brillouin zone. According to that, the expected behavior is that the gap closes and reopens as the sublattice asymmetry grows, going from the original topological phase to a trivial insulating phase.

To check this, we will compare the results obtained from the TB model

and DFT calculations. In the TB case, we introduce a new parameter which is a diagonal on-site energy whose value is $+m$ for A atoms and $-m$ for B atoms. This new parameter will break IS and its value will take into account the amount of breaking. When IS is broken the index ν cannot be calculated with the parities at the TRIM's. However, we can study the topological character searching for gapless edge states. For that sake we calculate the band structure of a zig-zag ribbon of 50 dimers width with $\alpha = t$ and $\lambda_{tri} = -t$. The calculations were also carried out in an armchair ribbon and the same behavior is found (not shown), however the mixing of valleys makes the band structure harder to understand. According to the result of the TB model shown in Fig. 3.10a and 6b, for small m the system remains a topological insulator although the introduction of m weakens the gap. If m keeps increasing the system reaches a critical point where the gap vanishes and if m increases even more the gap reopens but now the edge states became gapped so the system is in a trivial insulating phase.

To model the symmetry breaking in the DFT calculations we move one of the Pt atoms in the z direction. As the distance to the original point increases IS gets more broken. We show the four closest eigenvalues to the Fermi level in the K point for the DFT calculations (Fig. 3.10c) and TB model (Fig. 3.10d). For the symmetric structure ($\Delta z = 0$), the combination of TR and IS guarantees that each eigenvalue is two-fold degenerate. Once the atom is moved the degeneracy is broken and the eigenvalues evolve with the IS breaking parameter. The analog between the two calculations suggest that in the DFT calculation once the gap reopens the new state is also a trivial insulator. The dashed lines in Fig. 3.10c correspond to the eigenvalues at the K point for the fully relaxed structure allowing IS breaking. Comparing with the curves obtained for the evolution of the eigenvalues it is observed that the relaxed structure is in a slightly asymmetric configuration but it remains in the HUTI phase.

Due to the dependence of the topological state on IS, tuning this behavior would allow to make a device formed by a perovskite heterostructure which can be driven from a topological phase to a trivial phase applying a perpendicular electric field. The device will be formed by the TM honeycomb lattice sandwiched between layers of the same insulating (111) perovskite from above and below. In this configuration the system will be in a HUTI phase. However, a perpendicular electric field will break more the sublattice symmetry inducing a much greater mass term in the Hamiltonian proportional to the applied field. Modifying the value of the electric field it would be possible to drive the system from the topological phase ($\vec{E} = 0$), to the trivial phase (high $\vec{E}$). This can be exploited as an application of

this TI in nanoelectronic and spintronic devices.[65–68] The sublattice asymmetry needed to make the transition is in the same order of magnitude as the topological gap, as can be checked in Fig. 3.10a.

Chapter 4

Conclusions

We have studied the t_{2g}^5 perovskite multilayers $(SrTiO_3)_7/(SrIrO_3)_2$ and $(KTaO_3)_7/(KPtO_3)_2$ as a function of the on-site Coulomb interactions and uniaxial perpendicular strain conserving time reversal and inversion symmetry. The behavior of the system has been understood with a simple TB model where SOC gave rise to an effective j=1/2 four-band Hamiltonian. Uniaxial strain and on-site interactions have been identified as a trigonal term in the TB model whose strength controls the magnitude of a topological gap. The topological invariant ν has been calculated using the parities at the TRIM's both in TB and DFT calculations. Comparisons between the invariants of the bands determines that both of these 5d electron systems stay in the intermediate SOC regime. The small value of the gap in the K-point comes from being a contribution of third order in perturbation theory. In contrast, sublattice asymmetry contributes as a first order term, so the topological phase can be easily destroyed by an external perturbation that gives rise to an IS-breaking term in the Hamiltonian.

$(SrTiO_3)_7/(SrIrO_3)_2$ has been found to be a topological semimetal at equilibrium ϵ_{zz}. Comparing TB-mBJ and LDA+U calculations we have estimated the value of U in the Ir atoms as U-J=0.5 eV. In $(KTaO_3)_7/(KPtO_3)_2$ a HUTI phase at equilibrium has been found. In this system a perpendicular electric field could drive the topological insulating state to a trivial insulating state in a reversible way.

Although the smallness of the gap makes the t_{2g}^5 configuration not particularly attractive for technological applications, the simple understanding of the system turns it physically very interesting. The present system can be thought of as an adiabatic deformation of a mathematical realization of the four band graphene with SOC, with an experimentally accessible gap, the

roles of $\vec{S}$ and H_{SO} being played now by $\vec{J}_{eff}$ and H_{tri}, but with a different physical nature of the topological state.

Appendix A

Calculation methods

A.1 Tight binding model

Suppose we have a Hamiltonian of a one dimensional system with translation invariance. We split the system in identical neighbouring blocks and we choose a basis of localized orbitals in each of the blocks, in such a way an orbital in one block is the translation of an orbital in other block.

We take the following notation, in each block n, the ith local wavefunction is $|n,i\rangle$. We suppose orthogonality between orbitals $\langle m,j|n,i\rangle = \delta_{nm}\delta_{ij}$. To calculate the representation of the Hamiltonian we calculate the matrix elmentens in the basis of the previous orbitals. Taking into acount that we suppose that the Hamiltonian only mixes neighbouring cells, the elements needed are the following

Intracell hopping

$$\epsilon_{i,j}^{n,n} = \langle n,i|H|n,j\rangle \tag{A.1}$$

Intercell hopping

$$t_{i,j}^{n,n+1} = \langle n,i|H|n+1,j\rangle \tag{A.2}$$

$$t_{i,j}^{n+1,n} = \langle n+1,i|H|n,j\rangle = \langle n,j|H|n+1,i\rangle^* = t_{j,i}^{*n,n+1} \tag{A.3}$$

If T is the operator (T is an unitary operator so $TT^\dagger = I$) that make translation on the system then $|n+1,i\rangle = T|n,i\rangle$. If the system has translation invariance $T^\dagger HT = H$. Given the previous relations, one has that

$$\epsilon_{i,j}^{n,n} = \langle n,i|H|n,j\rangle = \langle n,i|T^\dagger HT|n,j\rangle = \langle n+1,i|H|n+1,j\rangle = \epsilon_{i,j}^{n+1,n+1} \tag{A.4}$$

$$t_{i,j}^{n,n+1} = \langle n,i|H|n{+}1,j\rangle = \langle n,i|T^\dagger HT|n{+}1,j\rangle = \langle n{+}1,i|H|n{+}2,j\rangle = t_{i,j}^{n+1,n+2} \tag{A.5}$$

so for every n the intracell elements of the Hamiltonian are equal, $\epsilon_{i,j}^{n,n} = \epsilon_{i,j}$, the hopping to the right cells are equal $t_{i,j}^{n,n+1} = t_{i,j}$ and the hopping to the left cell are equal as well (and the hermitian of previous one) $t_{i,j}^{n,n+1} = t_{j,i}^*$

The action over one local wavefunction of the Hamiltonian will be

$$H|n,i\rangle = \sum_j (\epsilon_{i,j}|n,j\rangle + t_{i,j}|n+1,j\rangle + t_{j,i}^*|n-1,j\rangle) \tag{A.6}$$

Now we define the following wavefunctions in spinorial form, where each component of the spinor is the local i-wavefunction

$$|n\rangle = \begin{pmatrix} |n,1\rangle \\ |n,2\rangle \\ |n,3\rangle \\ \vdots \end{pmatrix} \tag{A.7}$$

and the following matrices where their elements are the intracell and intercell hoppings

$$\epsilon = \{\epsilon_{i,j}\} \quad t = \{t_{i,j}\} \quad t^\dagger = \{t_{j,i}^*\} \tag{A.8}$$

with the previous notation, the action of the Hamiltonian on the spinors takes the simple form

$$H|n\rangle = \epsilon|n\rangle + t|n+1\rangle + t^\dagger|n-1\rangle \tag{A.9}$$

but keeping in mind that $|n\rangle$ is a spinor and ϵ,t are matrices. To diagonalize the previous Hamiltonian we define the normal modes (or Bloch states)

$$|k\rangle = \sum_n e^{i\phi n}|n\rangle \tag{A.10}$$

We have dropped the normalization factor for simplicity. Taking into account that

$$\sum_n e^{i\phi n}|n-1\rangle = e^{i\phi}\sum_n e^{i\phi n}|n\rangle = e^{i\phi}|k\rangle \tag{A.11}$$

given that we suppose an infinite system, it is easy to check that the action of the Hamiltonian on the previous states is diagonal

$$H|k\rangle = \sum_n e^{i\phi n} H|n\rangle = \sum_n e^{i\phi n}[\epsilon|n\rangle + t|n+1\rangle + t^\dagger|n-1\rangle] = [\epsilon + e^{-i\phi}t + e^{i\phi}t^\dagger]|k\rangle \tag{A.12}$$

so for each $|k\rangle$ the Hamiltonian is diagonal and takes the form

$$H|k\rangle = [\epsilon + e^{-i\phi}t + e^{i\phi}t^\dagger]|k\rangle \tag{A.13}$$

The phase ϕ is identified as $\phi = -\vec{k}\cdot\vec{a}$ where $\vec{k}$ is the a vector in the Brillouin zone and $\vec{a}$ is the lattice vector. For simplicity we take $\phi = -k$

The band structure is defined by the eigenvalues of the following matrix for each k

$$H_k = \epsilon + e^{ik}t + e^{-ik}t^\dagger \tag{A.14}$$

The generalization to higher dimensional models with hopping in combined directions is straighfoward. Reproducing the previous procedure for several hoppings and identifying the different phases with different points in the n-dimensional Brillouin zone the Hamiltonian takes the form

$$H_{\vec{k}} = \epsilon + \sum_n e^{i\vec{k}\cdot\vec{a}_n}t_n + e^{-i\vec{k}\cdot\vec{a}_n}t_n^\dagger \tag{A.15}$$

A.2 LAPW+lo method: The WIEN2k package

In order to solve theoretically the many body quantum mechanical problem of electrons in a certain crystal structure one has to solve the full Schrodinger equation. Due to the many body interactions its exact solution is unaproachable even computationally. To solve this point, the Hohenberg-Kohn theorem guarantees that the ground state of a system can be determined only by the electronic density, instead the general case of excited states where the full many body wavefunction is needed to characterize the system. However, such functional is unknown so the classic approach is to suppose a noninteracting system whose density is the same as the one of the real system but with a new Hamiltonian. This guess has another problem which is that the functional is still unknown, so to perform calculations one has to suppose a certain form of the functional. The terms of the energy supposed in the functional are the usual kinetic and Coulombic potential terms plus an additional exchange-correlation term whose form is unknown so certain approximations are employed as LDA, LDA+U or GGA. Once the functional

is chosen, the equations of motion are calculated in the usual way, obtaining the so called Kohn-Shan equations.

To solve the previous mean field nonlinear system a certain basis has to be chosen. The computational cost of the calculation depends both on the number of electrons considered and on the size of the basis chosen. The precision of the calculation depends on how well the restriction of the basis chosen reproduces the exact wavefunctions. The computational cost can be drastically reduced maintaining a good convergence by taking the adequate basis. The basis chosen in the present case will consist in augmented plane waves, i.e. plane waves in an interstitial region between atoms and radial times spherical harmonics near the atoms with the usual continuity boundary conditions, as implemented in the package WIEN2k.[53] To fufill this continuity, one has to restrict to a basis of maximun size in plane waves and spherical harmonics in sucha way the matching can be done in all the muffin thin sphere. Since the number of oscillations of the MT part is determined by the maximun order of $l_{\max}$ and the plane wave is $R_{\mathrm{mt}}K_{\max}$, so the correct scaling of the basis set will be of the form $R_{\mathrm{mt}}K_{\max} = l_{\max}$.

The problem of the previous method is that the basis depends on the energy and so the diagonalization will give an eigenfunction when the exact correct energy is taken at the beginning, so the selfconsistent solution has to be performed for each eigenvalue. Tha way to solve this problem is by upgraded the basis on the fly by a Taylor series and this is the so called linearized augmented plane wave (LAPW) method. The energies that should be chosen are the closest to the expected energies, i.e. close to p-bands for example, in order to have an accurate Taylor expansion to first order.

In order to describe semicore states (states which leak out the muffin tin sphere but have an n lower than the one should expect will have to consider) an addition of new vectors to the basis is useful. The new wavefunctions are called local orbitals and are defined radial times spherical harmonics but with vanishing boundary conditions in the MT sphere.

The spin-orbit coupling is taken into account in a second variational manner using the scalar relativistic approximation.

Bibliography

[1] J. E. Moore, Nature **464** 194–198 (2010).

[2] M. Z. Hasan and C. L. Kane, Rev. Mod. Phys. **82**, 3045 (2010).

[3] L. Fu, C. L. Kane, and E. J. Mele, Phys. Rev. Lett. **98**, 106803 (2007).

[4] D. Hsieh, Y. Xia, L. Wray, D. Qian, A. Pal, J. H. Dil, J. Osterwalder, F. Meier, G. Bihlmayer, C. L. Kane, et al., Science **323**, 919 (2009).

[5] Y. L. Chen, J. G. Analytis, J.-H. Chu, Z. K. Liu, S.-K. Mo, X. L. Qi, H. J. Zhang, D. H. Lu, X. Dai, Z. Fang, et al., Science **325**, 178 (2009).

[6] Y.-Y. Li, G. Wang, X.-G. Zhu, M.-H. Liu, C. Ye, X. Chen, Y.-Y. Wang, K. He, L.-L. Wang, X.-C. Ma, et al., p. arXiv:0912.5054 (2009).

[7] H.-M. Guo and M. Franz, Phys. Rev. B **81**, 041102 (2010).

[8] R. R. Biswas and A. V. Balatsky, Phys. Rev. B **83**, 075439 (2011).

[9] X. Zhou, C. Fang, W.-F. Tsai, and J. Hu, Phys. Rev. B **80**, 245317 (2009).

[10] A. M. Essin and V. Gurarie, Phys. Rev. B **84**, 125132 (2011).

[11] D. J. Thouless, M. Kohmoto, M. P. Nightingale, and M. den Nijs, Phys. Rev. Lett. **49**, 405 (1982).

[12] C. L. Kane and E. J. Mele, Phys. Rev. Lett. **95**, 146802 (2005).

[13] A. Altland and M. R. Zirnbauer, Phys. Rev. B **55**, 1142 (1997).

[14] D. N. Sheng, Z. Y. Weng, L. Sheng, and F. D. M. Haldane, Phys. Rev. Lett. **97**, 036808 (2006).

[15] E. Prodan, Journal of Physics A: Mathematical and Theoretical **42**, 082001 (2009).

[16] B. A. Bernevig, T. L. Hughes, and S.-C. Zhang, Science **314**, 1757 (2006).

[17] Shun-Qing Shen Topological Insulators ISBN: 978-3-642-32857-2

[18] J. Zak 1989 Europhys. Lett. 9 615

[19] Hideo Aoki, Tsuneya Ando, Phys. Rev. Lett. 57, 3093-3096 (1986)

[20] Di Xiao, Ming-Che Chang, Qian Niu, Rev. Mod. Phys. 82, 1959-2007 (2010)

[21] Emil Prodan Phys. Rev. B 80, 125327 (2009)

[22] Norman Y. Yao, Chris R. Laumann, Alexey V. Gorshkov, Hendrik Weimer, Liang Jiang, J. Ignacio Cirac, Peter Zoller, Mikhail D. Lukin, Nature Communications 4,1585

[23] M. Knig, S. Wiedmann, C. Brne, A. Roth, H. Buhmann, L. W. Molenkamp, X.-L. Qi, and S.-C. Zhang, Science **318**, 766 (2007).

[24] K. C. N. et al., arXiv:1212.2203 (2012).

[25] C.-C. Liu, W. Feng, and Y. Yao, Phys. Rev. Lett. **107**, 076802 (2011).

[26] D. Xiao, W. Zhu, Y. Ran, N. Nagaosa, and S. Okamoto, Nature Communications **2**, 596 (2011).

[27] L. Fu and C. L. Kane, Phys. Rev. B **76**, 045302 (2007).

[28] R.Jackiw and C.Rebbi, Phys. Rev. D 13, 3398 (1976)

[29] Shun-Qing Shen, Wen-Yu Shan, Hai-Zhou Lu, arXiv:1009.5502

[30] W. P. Su, J. R. Schrieffer, and A. J. Heeger, Phys. Rev. Lett. 42, 1698-1701 (1979)

[31] F. D. M. Haldane, Phys. Rev. Lett. 61, 2015-2018 (1988)

[32] C. L. Kane and E. J. Mele, Phys. Rev. Lett. 95, 226801 (2005)

[33] Y. Yao, F. Ye, X.-L. Qi, S.-C. Zhang, and Z. Fang, Phys. Rev. B **75**, 041401 (2007).

[34] M. Topsakal, E. Aktürk, and S. Ciraci, Phys. Rev. B **79**, 115442 (2009).

[35] G. Giovannetti, P. A. Khomyakov, G. Brocks, P. J. Kelly, and J. van den Brink, Phys. Rev. B **76**, 073103 (2007).

[36] A. Rüegg and G. A. Fiete, Phys. Rev. B **84**, 201103 (2011).

[37] K.-Y. Yang, W. Zhu, D. Xiao, S. Okamoto, Z. Wang, and Y. Ran, Phys. Rev. B **84**, 201104 (2011).

[38] F. Wang and Y. Ran, Phys. Rev. B **84**, 241103 (2011), .

[39] A. Rüegg, C. Mitra, A. A. Demkov, and G. A. Fiete, Phys. Rev. B **85**, 245131 (2012), .

[40] S. Okamoto, Phys. Rev. Lett. **110**, 066403 (2013).

[41] F.-X. Wu, J. Zhou, L. Y. Zhang, Y. B. Chen, S.-T. Zhang, Z.-B. Gu, S.-H. Yao, and Y.-F. Chen, Journal of Physics: Condensed Matter **25**, 125604 (2013), .

[42] S. J. Moon, H. Jin, K. W. Kim, W. S. Choi, Y. S. Lee, J. Yu, G. Cao, A. Sumi, H. Funakubo, C. Bernhard, et al., Phys. Rev. Lett. **101**, 226402 (2008).

[43] M. Schmidbauer, A. Kwasniewski, and J. Schwarzkopf, Acta Crystallographica Section B **68**, 8 (2012), .

[44] J. Narkilahti and M. Tyunina, Journal of Physics: Condensed Matter **24**, 325901 (2012), .

[45] A. Shitade, H. Katsura, J. Kuneš, X.-L. Qi, S.-C. Zhang, and N. Nagaosa, Phys. Rev. Lett. **102**, 256403 (2009).

[46] S. J. Moon, H. Jin, K. W. Kim, W. S. Choi, Y. S. Lee, J. Yu, G. Cao, A. Sumi,H. Funakubo, C. Bernhard, and T. W. Noh, Phys. Rev. Lett. 101, 226402 (2008)

[47] Cyril Martins, Markus Aichhorn, Log Vaugie1, and Silke Bierman,Phys. Rev. Lettt . 107, 266404 (2011)

[48] R. Arita, J. Kune, A. V. Kozhevniko, A. G. Eguilu, and M. Imad, Phys. Rev. Lett. 108, 086403 (2012)

[49] Christoph Loschen, Javier Carrasco, Konstantin M. Neyman, and Francesc Illas Phys. Rev. B 75, 035115 (2007)

[50] R. Comin, G. Levy, B. Ludbrook, Z.-H. Zhu, C. N. Veenstra, J. A. Rosen, Y. Singh, P. Gegenwart, D. Stricker, J. N. Hancock, et al., Phys. Rev. Lett. **109**, 266406 (2012).

[51] S. Raghu, X.-L. Qi, C. Honerkamp, and S.-C. Zhang, Phys. Rev. Lett. **100**, 156401 (2008).

[52] L. B. Dmytro Pesin, Nature Physics **6**, 376 (2010).

[53] K. Schwarz and P. Blaha, Comp. Mat. Sci. **28**, 259 (2003).

[54] J. P. Perdew, K. Burke, and M. Ernzerhof, Phys. Rev. Lett. **77**, 3865 (1996).

[55] V. I. Anisimov, J. Zaanen, and O. K. Andersen, Phys. Rev. B **44**, 943 (1991).

[56] F. Tran and P. Blaha, Phys. Rev. Lett. **102**, 226401 (2009).

[57] D. J. Singh, *Planewaves, pseudopotentials and LAPW method* (Kluwer Academic Publishers, 1994).

[58] X. Wan, A. M. Turner, A. Vishwanath, and S. Y. Savrasov, Phys. Rev. B **83**, 205101 (2011).

[59] Andreas Fuhrmann, David Heilmann, and Hartmut Monien, Phys. Rev. B 73, 245118 (2006)

[60] S. S. Kancharla and S. Okamoto, Phys. Rev. B 75, 193103 (2007)

[61] D. J. Singh, Phys. Rev. B **82**, 205102 (2010).

[62] H. Jiang, American Institute of Physics **138**, 134115 (2013).

[63] A. S. Botana, F. Tran, V. Pardo, D. Baldomir, and P. Blaha, Phys. Rev. B **85**, 235118 (2012).

[64] J. B. Goodenough, *Magnetism and the chemical bond* (IEEE Press, New York, 2001).

[65] P. Michetti and B. Trauzette, Applied Physics Letters **102**, 063503 (2013).

[66] Y. T. M. P. G. K. Parijat Sengupta, Tillmann Kubis, arXiv:1302.5716 (2013).

[67] Romeo, F., Citro, R., Ferraro, D., Sassetti, and M., Phys. Rev. B **86**, 165418 (2012).

[68] H. Zhu, C. A. Richter, E. Zhao, J. E. Bonevich, W. A. Kimes, H.-J. Jang, H. Yuan, H. Li, A. Arab, O. Kirillov, et al., Scientific Reports **3** (2013).